3.1. Introduction

A large number of Cu(II) complexes with a variety of O,N donor ligands are reported every year. [1-3]

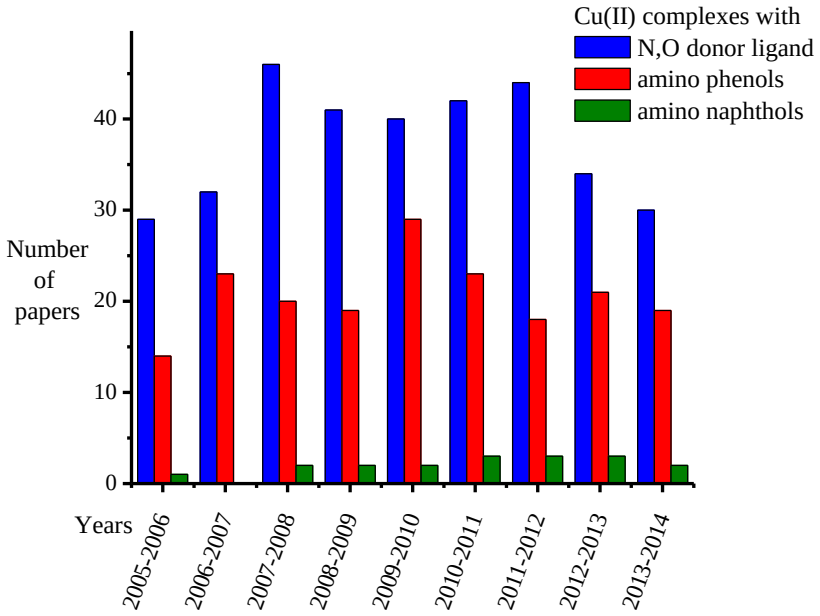

Figure 3.1 The number of papers concerning the Cu(II) complex with (blue) N,O donor ligands, (red) amino phenols and (green) amino naphthols being published within 2005-2014 (Data taken from Thompson Reuters)

Most of this research is inspired by biological systems, wherein these complexes can mimic various roles of metalloproteines like activation of dioxygen, electron transfer and transport.[4] Synthesis and study of redox properties of Cu(II) complexes with derivatives of aminophenols have attracted attention of many scientists as these can act as model for Galactose oxidase (GAO), whose copper(II)-phenoxyl radical is found to be a key reactive intermediate for the two-electron oxidation of primary alcohols to aldehydes. [5-7]

It is reveled through structural, spectroscopic, and kinetic studies that the reaction catalyzed by GAO involves electron transfer through copper ion (CuI/CuII) and coordinated tyrosinate that is oxidized to a tyrosyl radical during catalytic cycle (Scheme 3.1). [8,9]

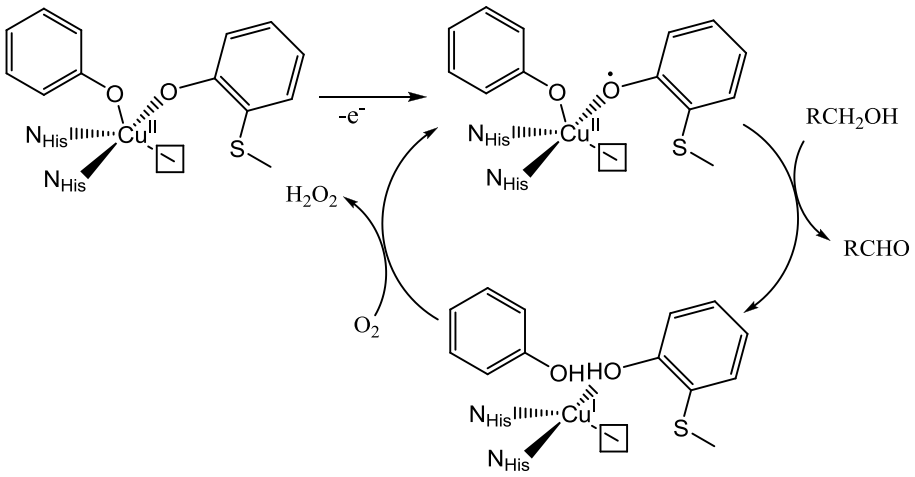

Scheme 3.1 Mechanism of oxidation by GAO

Though a large number of Cu(II) complexes that mimic the role of GAO are reported only few examples are incorporated here.

Several research groups have reported Cu(II) complexes with the ligands that have in common, pyridyl alkylamines linked to a phenol. (Fig. 3.2) [10]

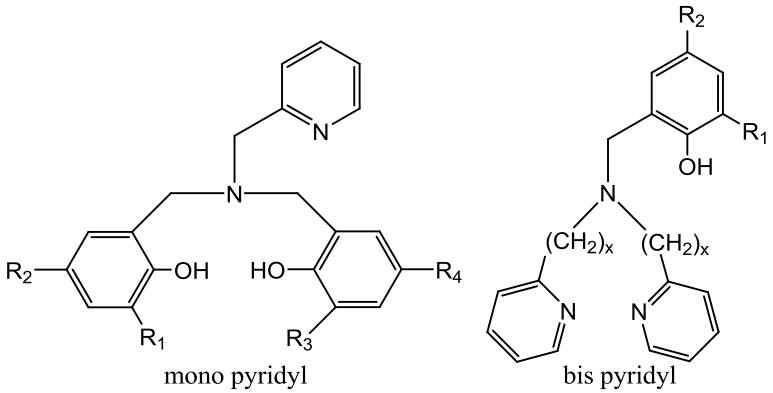

Figure 3.2 Mono and bis(pyridyl)alkylamine ligands

Cu (II) complexes with three secondary amino groups of triazacyclononanes (TACN) incorporated in substituted phenols have been reported by Wieghardt et al. [11] (Fig. 3.3)

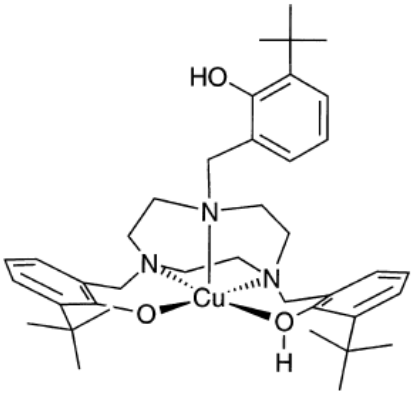

Figure 3.3 Schematic representation of the structure of the mixed Cu(II)–phenolate/phenol complex [11]

A large number of Cu(II) complexes with SALEN frame have been reported as these complexes with appropriate substitution provide tetrahedral distortion around central Cu(II), which has been proved to be important in stabilizing Cu(I) providing a better model mimicking the oxidase activity by facilitating substrate binding during catalysis process. [12-15]

Another class of Cu (II) complexes that has been proposed as model for GAO based on hydrotris(pyrazolyl)borates. The hydrotris(pyrazolyl)borate ligand (Tp^R) mainly consist of histidine-like N-donors and pyrazolyl substituents. [16] The presence of two available coordination sites in Tp^R complexes of Cu(II) can be filled with exogenous bidentate, phenolate-containing ligands. The resulting five-coordinate, square pyramidal Cu(II) complexes have been suggested to be structural models of GAO. (Fig. 3.4)

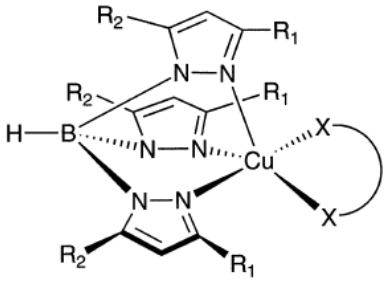

Figure 3.4 Schematic representation of Tp^RCu(II)(phenolate) complexes, where X = a exogenous, bidentate phenolate ligand (R_1 = R_2 = alkyl substituents).

Apart from the above mentioned classes of Cu(II) complexes, in the past decade, Weighardt et al. and others have published valuable reports of spectroscopic and functional models of GAO based on noninnocent Cu complexes of aminophenol ligands.[1a, 7, 17, 18, 19]

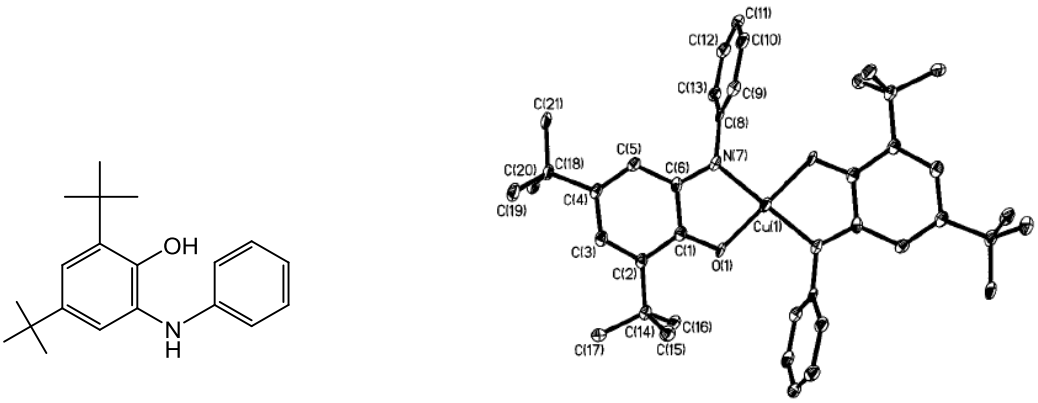

Figure 3.5 Structure of 2-Anilino-4,6-di-*tert*butylphenol and its Cu(II) complex

Garner et al. [19e] have synthesized the Cu(II) complexes with 2-[2'-(4',6'-di-*tert*butylhydroxyphenyl)]- 4,5-diphenylimidazole.

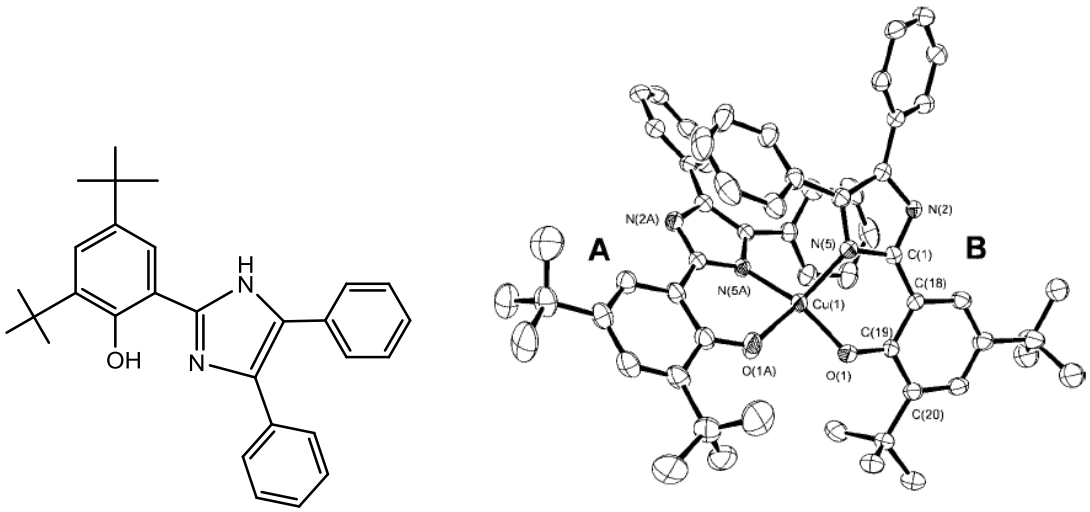

Figure 3.6 Structure of 2-[2'-(4',6'-di-*tert*butylhydroxyphenyl)]- 4,5-diphenylimidazole and its Cu(II) complex

Thomas et al. [7e] have strategically synthesized the tripodal amino phenol ligand (Fig. 3.7) to allow the geometric control of the one electron oxidized active form of Cu(II) complex. [1a]

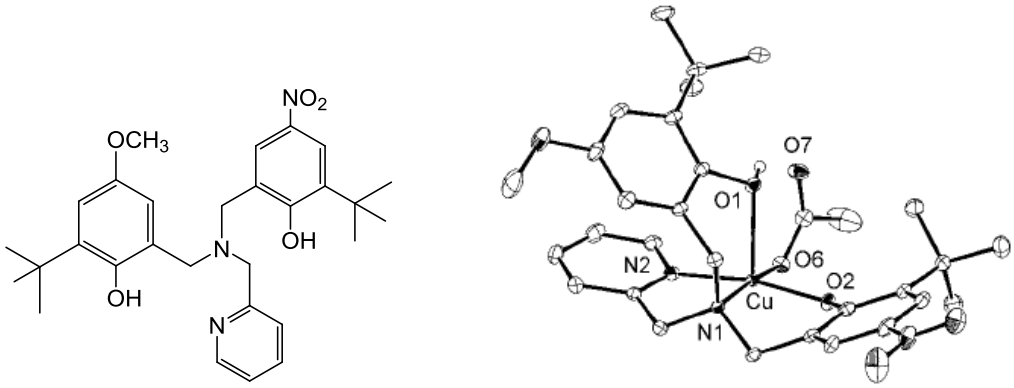

Figure 3.7 Structure of tripodal amino phenol and its Cu(II) complex

Chaudhuri et al. [19c] have synthesized bis(o-iminosemiquinonato)copper(II) complexes derived from differently substituted N-phenyl-2-amino phenol based ligands (Fig. 3.8)

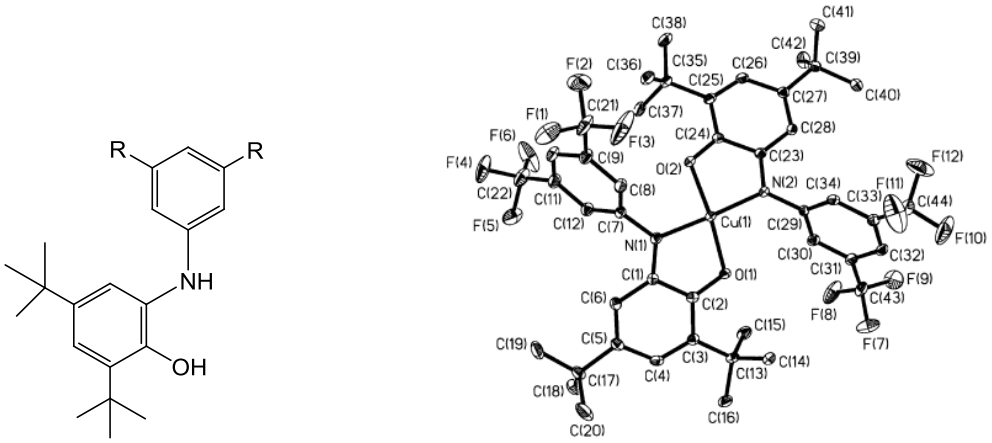

Figure 3.8 Structure of N-Phenyl-2-amino phenol substituted ligand and its Cu(II) complexes

On the basis of cyclic voltammetric study and the results obtained from single crystal X-ray analysis, DFT, EPR analysis, the electrochemically generated different redox species for the Cu(II) complex have been proposed. (Scheme 3.2)

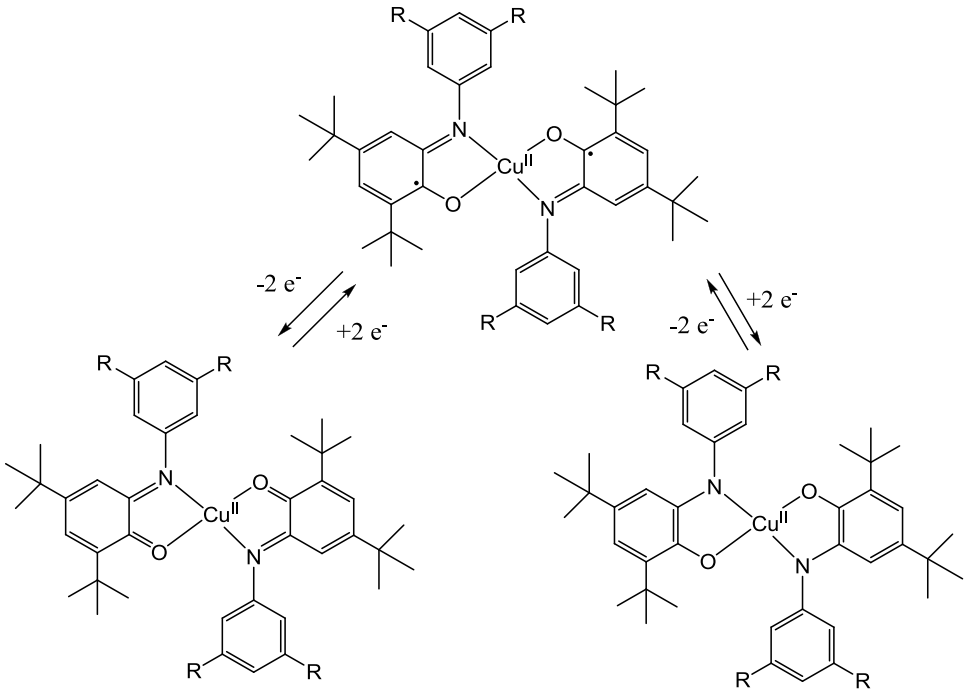

Scheme 3.2 Electrochemically generated different redox states for Cu(II) complex

Recently Storr et al. [19g, 20] have synthesized and used as catalyst Cu(II) complexes with redox active benzoxazole iminosemiquinone ligand and iminophenol amidopyridine ligand for aerobic oxidation of alcohols. (Fig. 3.9)

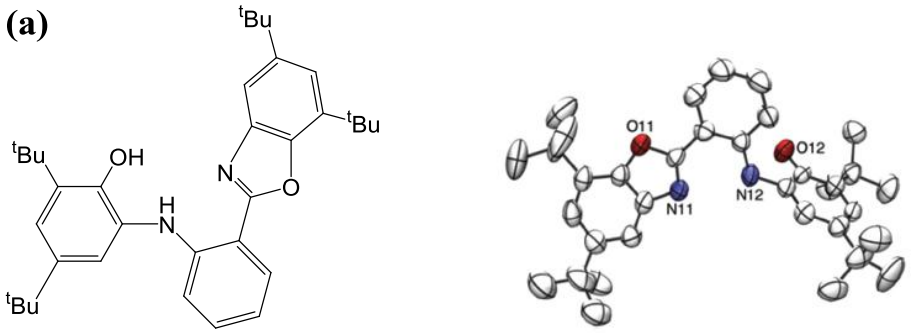

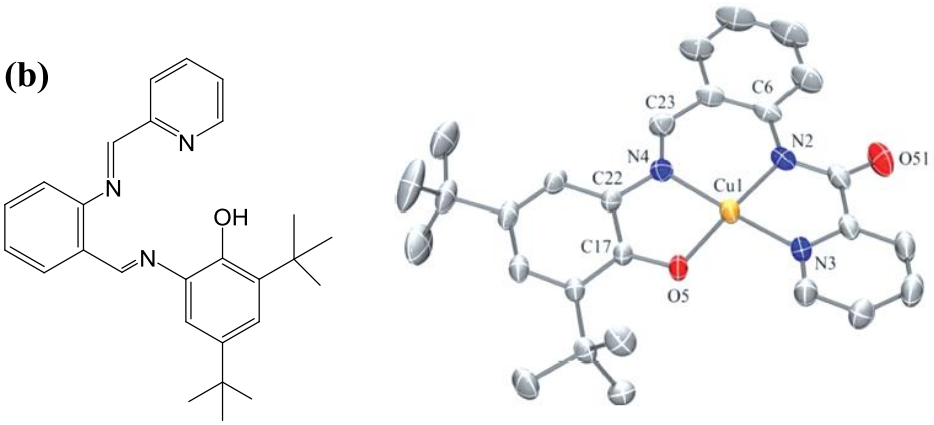

Figure 3.9 Structures of (a) benzoxazole iminosemiquinone ligand and its Cu(II) complex (b) iminophenol amidopyridine ligand and its Cu(II) complex

So far, most of the research work has been reported on the redox active amino phenol ligands and their Cu(II) complexes. Synthesis of Cu(II) complexes with BB and their redox properties have not been reported so far.

Optically active Betti bases complexed to dialkyl zinc have been used for enantioselective addition to aryl aldehydes. Various applications of enantiopure amino naphthols as catalyst in stereoselective reactions have been reviewed by Ferenc Fulop et al. and Gianni Palmieri et al. [21,22] It is evident that, to understand the role of Betti base in ligand accelerated reactions in presence of metal salt, isolation and characterization of the metal complex is essential.

Betti base, with $–NH_2$ and –OH groups at 1 and 3 positions respectively, is expected to act as an excellent ligand for coordination with transition metal ion. In this light Cu(II) complexes with Betti bases have been synthesized and characterized.

3.2. Experimental

3.2.1. Materials

Freshly distilled solvents were employed for all synthetic purposes. Spectroscopic grade solvents were employed for spectral work. All other chemicals used were of AR grade.

3.2.2. Synthesis of Cu(II) complexes with Betti bases

The copper(II) complexes were prepared by mixing 2 mM solution of ligand in methanol with 1 mM methanolic solution of $CuCl_2 \cdot 2H_2O$ (scheme 3.3). The mixture was stirred for 30 min at room temperature. The solid separated from the solution was collected on a Whatman filterpaper, washed with small amount of methanol and dried under vacuum. Purity of the isolated complex was confirmed by TLC,(Hexane:ethyl acetate; 5:1). No unreacted ligand was found.

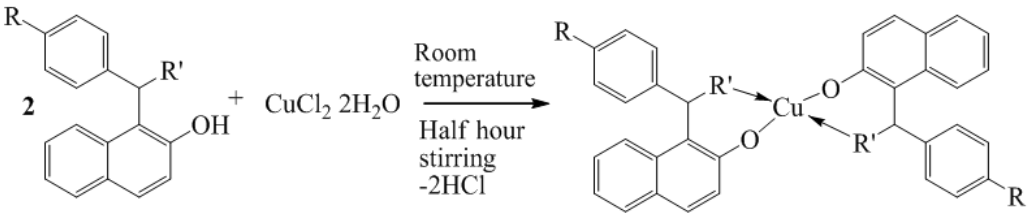

L_1 : R = H , R' = $-NH_2$
L_2 : *S* form of L_1
L_3 : *R* form of L_1
L_4 : R = H , R' = Pyrrolidine
L_5 : *S* form of L_4
L_6 : *R* form of L_4
L_7 : R = H, R' = $-N(CH_3)_2$
L_8 : R = $-OCH_3$, R' = $-NH_2$
L_9 : R = -OCH3, R' = $-N(CH_3)_2$

Cu1 : Cu (L_2 - H) (L_3-H)
Cu2 : Cu (L_2 – H)$_2$
Cu3 : Cu (L_3 – H)$_2$
Cu4 : Cu (L_5 – H) (L_6-H)
Cu5 : Cu (L_5 – H)$_2$
Cu6 : Cu (L_6 – H)$_2$
Cu7 : Cu (L_7 – H)$_2$
Cu8 : Cu (L_8 – H)$_2$
Cu9 : Cu (L_9 – H)$_2$

Scheme 3.3 Synthesis of Cu(II) Betti base complexes

3.2.3. Characterization of Cu(II) Betti base complexes

The Copper(II) complexes with Betti base and its derivatives were characterized by elemental analysis, thermal gravimetric analysis and various spectral techniques like FT-IR, UV-Visible, CD, FAB-Mass, EPR, and single crystal X-Ray analysis.

3.2.3.1. Elemental Analysis (C,H,N, Cu)

Elemental analysis (C,H,N) of the complexes were done on VARIO EL-III elemental analyzer. ICP-OES analysis for the estimation of metal was done using Thermo scientific iCAP 6200 ICP-OES.

3.2.3.2. Thermo Gravimetric analysis (TGA)

Thermal analysis of the complexes was done on SII TG/DTA 6300. Nitrogen gas was purged with the rate of 100 mL/min and the temperature was programmed in the range of 35-550 °C or 750 °C with the ramp of 10°C/min.

3.2.3.3. FT-IR

FT-IR spectra were recorded on Perkin Elmer RX1 Spectrometer by making KBr pellet of the compound.

3.2.3.4. Electronic spectra

UV–Vis spectra of the Cu(II) Betti base complexes (5 mM solution in chloroform) were recorded on a Perkin Elmer Lambda 35 UV–Vis spectrometer.

3.2.3.5. CD spectra

The CD spectra of 0.5 mM solution of the optically pure complexes (**Cu2,Cu3,Cu5,Cu6**) in chloroform were recorded using a Jasco J-810 Spectro-polarimeter in the range 250–800 nm.

3.2.3.6. FAB-Mass

Fast atomic bombardment mass spectra (FAB–Mass) were recorded on Jeol SX 102/Da-600 mass spectrometer using m-nitro benzyl alcohol as matrix.

3.2.3.7. EPR spectra

X-band EPR spectra were obtained on a Varian E-112 ESR spectrometer.

3.2.3.8. Single crystal X-Ray analysis (XRD)

X-ray diffraction data of **Cu1** complex were collected on a Bruker SMART APEX diffractometer equipped with CCD detector, using graphite-monochromatized Mo-K_α radiation (λ = 0.71073 Å) at 298^o K. The structure was solved by direct methods using SHELXTL [23] and was refined on F^2 by the full-matrix least-squares technique using the SHELXL-97 [24] program package.

3.2.4. Electrochemical analysis

Cyclic voltammetric study of the 0.005 M solution of Cu(II) complexes in DCM were carried out on a CH Instruments 600C potentiostat, with a glassy carbon as working electrode (area 0.071 cm^2), Ag/Ag^+ reference electrode (0.01 M $AgNO_3$ in acetonitrile) and Pt wire as a counter electrode. To obtain reproducible results, the glassy carbon electrode was polished using polishing kit (CHI120) which consisted of a polishing polyurethane pad, α–Al_2O_3 (particle size 1.0 & 0.3 μm) and gamma Al_2O_3 powder (particle size 0.05 μm). The electrode was polished with 0.05 μm alumina, sonicated (ultrasound bath) for 3 min and finally rinsed with deionized water before each measurement. Solutions were deoxygenated by bubbling dry nitrogen prior to the potential sweep. All experiments were carried out at room temperature.

3.3. Results and Discussion

3.3.1. Elemental analysis

To establish metal: ligand stoichiometry, elemental analysis (C,H,N) of the metal complexes was done. The theoretical values of C, H & N elements for 1:2 metal to ligand stoichiometry are matching with the experimental values. (Table 3.1)

Sr.No.	Complex	% C	% H	% N	% Cu
1	**Cu1**	72.33 (72.8)	5.01 (4.99)	4.85 (4.99)	
2	**Cu2**	72.50 (72.8)	4.89 (4.99)	4.99 (4.99)	11.29 (11.30)
3	**Cu3**	72.16 (72.8)	4.89 (4.99)	4.87 (4.99)	
4	**Cu4**	75.08 (75.48)	5.83 (6.03)	4.02 (4.19)	
5	**Cu5**	75.30 (75.48)	5.90 (6.03)	3.99 (4.19)	9.48 (9.51)
6	**Cu6**	75.18 (75.48)	5.89 (6.03)	4.08 (4.19)	
7	**Cu7**	73.84 (74.06)	5.67 (5.89)	4.16 (4.55)	10.28 (10.31)
8	**Cu8**	68.80 (69.72)	5.05 (5.20)	4.18 (4.52)	10.24 (10.25)
9	**Cu9**	69.81 (71.04)	5.41 (5.96)	3.92 (4.14)	9.38 (9.40)

Table 3.1 Elemental analysis of Cu(II) complexes with Betti bases; the theoretical value are shown in bracket.

3.3.2. Thermo Gravimetric Analysis

Thermal analysis of the complexes **Cu1**, **Cu4, Cu7, Cu8 & Cu9** in N_2 flow indicates complexes to be anhydrous and unsolvated [Fig. 3.10(a-e)]. No weight loss was observed until decomposition which began at about 220°C for **Cu1**, 232°C for **Cu4**, 209°C for **Cu7**, 230°C for **Cu8** and 215°C for **Cu9**.

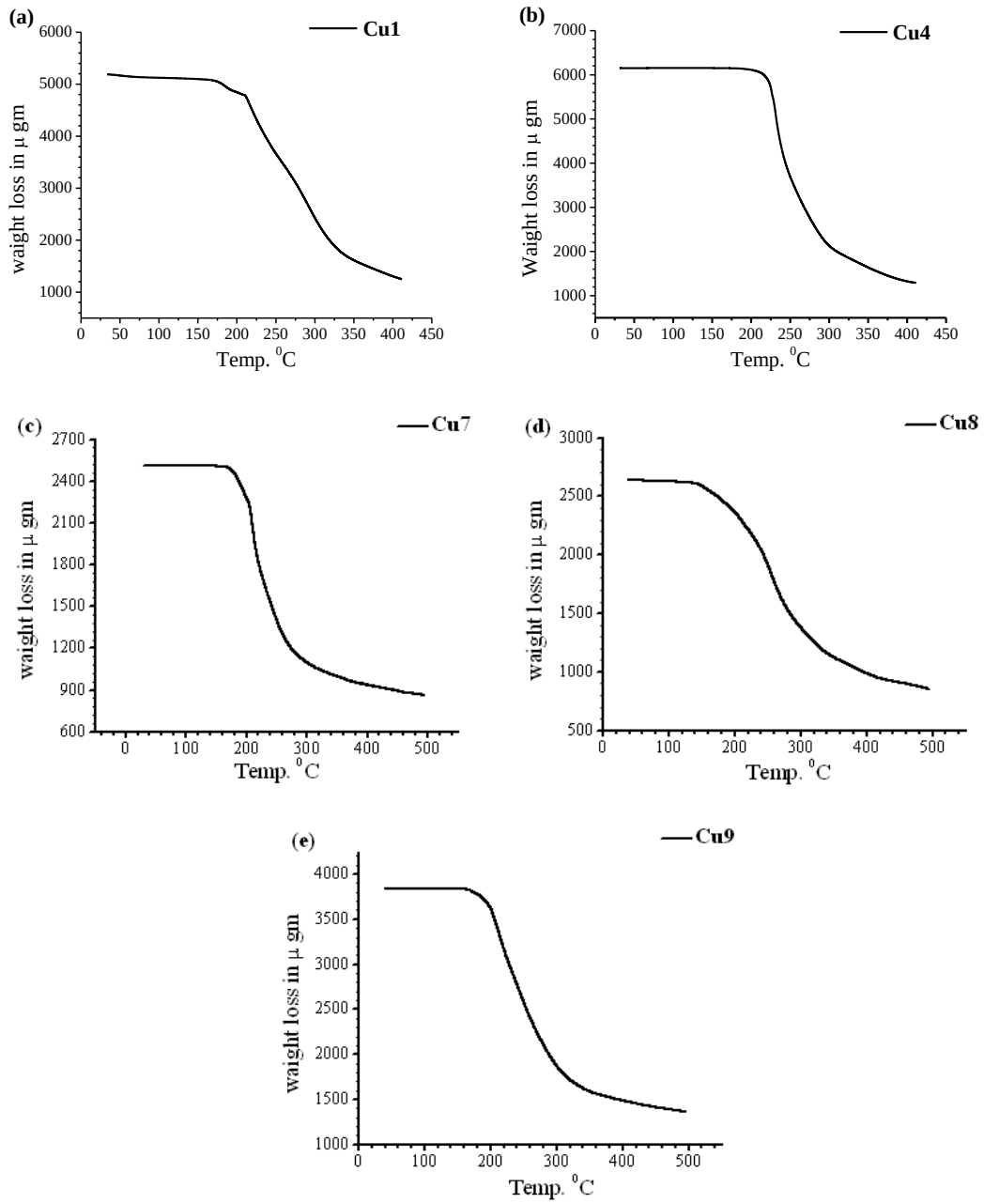

Figure 3.10 (a) TGA of **Cu1 (b)** TGA of **Cu4 (c)** TGA of **Cu7 (d)** TGA of **Cu8 (e)** TGA of **Cu9**

3.3.3. FT-IR

In IR spectra of the complexes **Cu1**, **Cu2** and **Cu3**, the band due to –OH stretching disappeared whereas two bands of $–NH_2$ stretching are shifted to slightly higher wave numbers, at 3439 cm^{-1} and 3341 cm^{-1}. (SI; Fig. 3.1SI) This shift indicates absence of H-bond and a very weak coordination bond between $–NH_2$ and copper (II) ion. [25] The band due to –OH stretching is not seen in the IR spectra of the complexes **Cu4**, **Cu5** and **Cu6** and the bands of –C-H and –C-N are shifted to 8-10 cm^{-1} higher wave numbers. These small shifts can be attributed to small changes on coordination with metal ion.

3.3.4. UV-Visible spectral analysis

The electronic spectra (Fig 3.11a) of complexes (**Cu3**, **Cu6**) 0.1 mM in chloroform exhibited slightly broad, more intense, intraligand transition bands at ~ 290 nm with extinction coeffiecient 8580 and at ~ 337 nm with extinction coefficient 6300 as expected for a coordinated phenoxo ligand with a metal ion. Apart from these intense bands, the spectra of complexes (**Cu1**, **Cu2**, **Cu3**) exhibited a band at ~ 360 nm with extinction coefficient 1800, which can be attributed to phenoxo ligand to metal charge transfer. A broad band, appeared at ~ 650 nm with extinction coefficient 164 for complexes with optically active ligands **Cu2** and **Cu3** (Fig 3.11b, 5 mM in chloroform), which can be assigned to d-d transition as expected for a Cu(II) square planar complex and can be attributed to a combination of three transitions $B_{1g} \rightarrow A_{1g}$, $B_{1g} \rightarrow B_{2g}$, $B_{1g} \rightarrow E_g$.

Similarly, a broad band at ~ 510 nm with extinction coefficient ~ 450, for **Cu5** – **Cu6** (Fig. 3.11b) can be assigned to d-d transition. The shift in d-d transition towards lower wavelength values compared with that of **Cu2** and **Cu3** complexes indicates more distorted tetragonal geometry around the central metal ion. This is expected for ligands bearing a bulkier group like pyrollidine. A similar shift has been observed by Elias et al.[26]

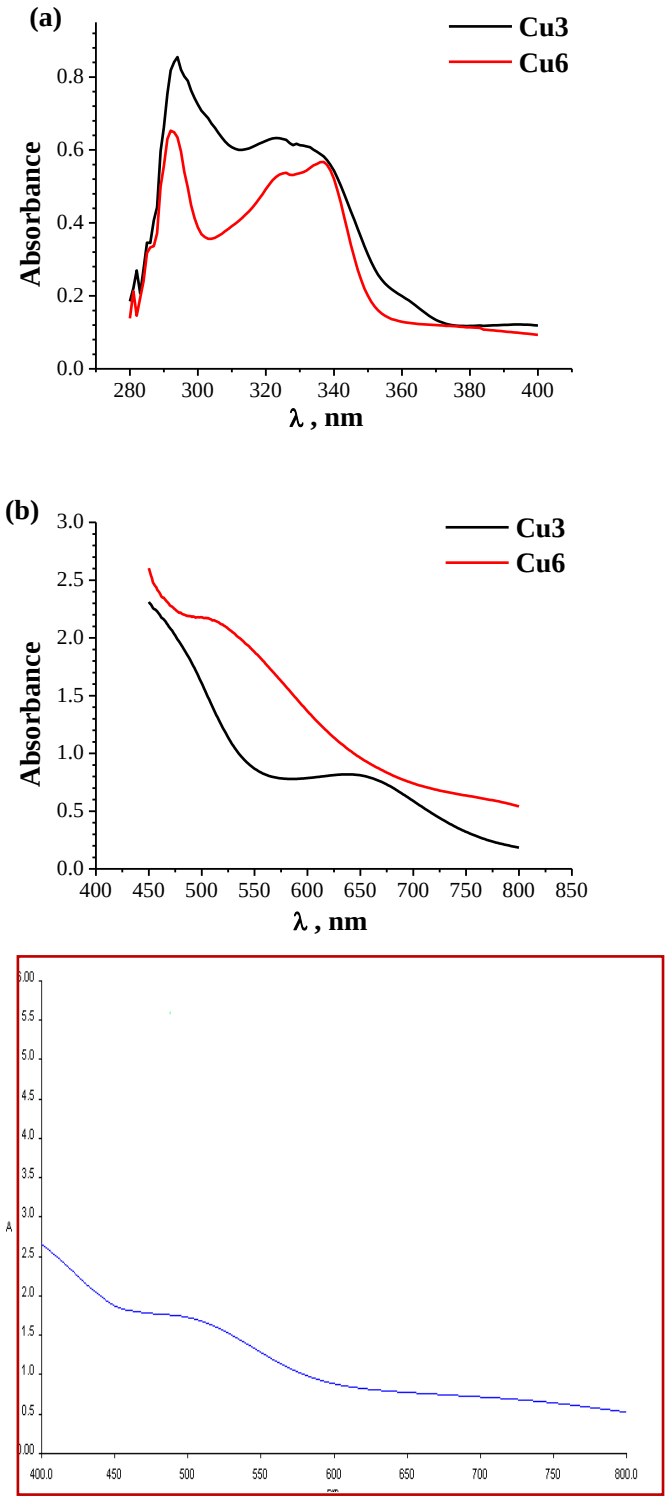

Figure 3.11 (a) UV spectra of **Cu3 & Cu6** (b) Visible spectra of **Cu3**, **Cu6 & Cu7**

3.3.5. Circular Dichroism spectra

The CD spectra of the chiral ligand derived complexes i.e. **Cu2** & **Cu3** and **Cu5** & **Cu6** are given in Figure 3.12 (a),(b). They are like ligands, mirror images of each other. However, the bands corresponding to intraligand transitions in the 280 nm to 305 nm cannot be reported due to high HT values. The band at 340 nm is observed with Cotton effect similar to that of corresponding ligands. Incorporation of metal ion [**Cu2** and **Cu3**] resulted in exhibition of charge transfer at ~ 388 nm with Cotton effect similar to that of corresponding ligand and a d-d transition band at ~ 670 nm of lower intensity but with reversal of Cotton effect.

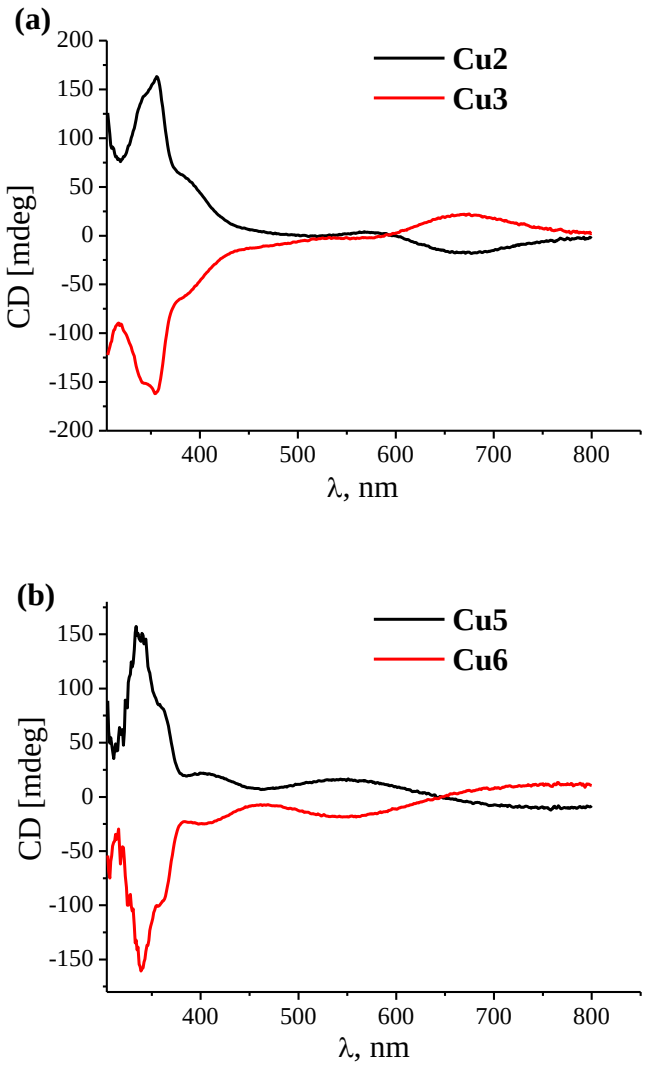

Figure 3.12 Circular Dichroism spectra (0.5mM) in 10mL of chloroform (a) CD spectra of **Cu2** and **Cu3** (b) CD spectra of **Cu5** and **Cu6**

The reversal of Cotton effect for d-d transition band could be explained considering coupling of d-d transitions either with one of the $\pi \rightarrow \pi^*$ transitions. Similar type of opposite Cotton effects resulted from exciton coupling have been reported. [27,28] The CD spectra of **Cu5** and **Cu6** are different from that of **Cu2** and **Cu3**. In case of **Cu5** and **Cu6**, charge transfer bands appeared at lower energies ~ 408 nm with Cotton effect similar to that of corresponding ligands, In contrast to the absorption spectra, CD spectra of the complexes exhibited two bands with opposite Cotton effects in 400 nm- 800 nm range. The band at 550 nm can be assigned to the combination of $B_{1g} \rightarrow B_{2g}$, $B_{1g} \rightarrow E_g$ d-d transitions and one at 760 nm can be assigned to $B_{1g} \rightarrow A_{1g}$ transition. This observation indicated a different geometry around Copper metal center in **Cu5** and **Cu6** than in **Cu2** and **Cu3**. Either strong ligand field or bulkiness of the substituent caused splitting of the three merged bands in to two bands. However, the $B_{1g} \rightarrow A_{1g}$ transition being very weak, it is not observed in the electronic absorption spectra.

3.3.6. FAB-Mass analysis

The 1:2 Metal to ligand stoichiometry of the Cu(II) complexes with Betti bases are further confirmed by FAB-Mass analysis. (SI; Fig. 3.2SI) FAB mass spectra of the complexes displayed molecular ion peaks corresponding to $[Cu(L\text{-}H)_2]^+$ ion confirming formation of the $Cu(L\text{-}H)_2$ complexes.

3.3.7. EPR analysis

The EPR spectra of all the complexes exhibited a good hyperfine splitting (Fig. 3.13) and corresponding $g_{\|}$, $g_{\perp}$ and $A_{\|}$ values are tabulated in Table 3.2. A distorted tetragonal geometry around copper ion is evident from $g_{II} > g_{\perp} > 2$ with $d_{x^2-y^2}$ ground state, as expected for a square planar copper(II) complex. [29] For a copper(II) complex, $g_{\|}$ parameter is sensitive enough to indicate covalance. It is known that [30] for a covalent Cu(II) complex, $g_{\|} < 2.3$, and for an ionic environment, normally $g_{\|} = 2.3$ or more. From the values of $g_{\|}$ (Table 3.2), a more covalent character is predicted for **Cu2**, **Cu3**, **Cu5** and **Cu6**, a less covalent environment around metal in **Cu4** and ionic character of bond around **Cu1**. The values of α^2 calculated using equation $\alpha^2 = -(A/0.036) + (g_{\|} - 2) + (3/7)(g_{\perp} - 2) + 0.04$, are given in Table 3.2. The values of α^2 greater than 0.5 are reported to indicate a more ionic character of the bond between

metal and the coordinating atom of the ligand. [31] In the present study, the α^2 values of all the complexes are larger than 0.5 indicating some ionic character of the Cu(II) – N and Cu(II) – O bonds. A close look at the magnitude of α^2 values reveals significant differences, like it is 0.715 for **Cu2** & **Cu3** and 0.86 for **Cu1**, suggesting a less ionic character of the metal ligand bond in **Cu2** & **Cu3** compared to that in **Cu1**. Thus, both $g_{\parallel}$ and α^2 values point to a different environment around Cu(II) ion, in **Cu1** and **Cu2** or **Cu3** despite of coordinated to chemically identical ligands. This signifies a more distorted arrangement of optically active ligands around metal ion.

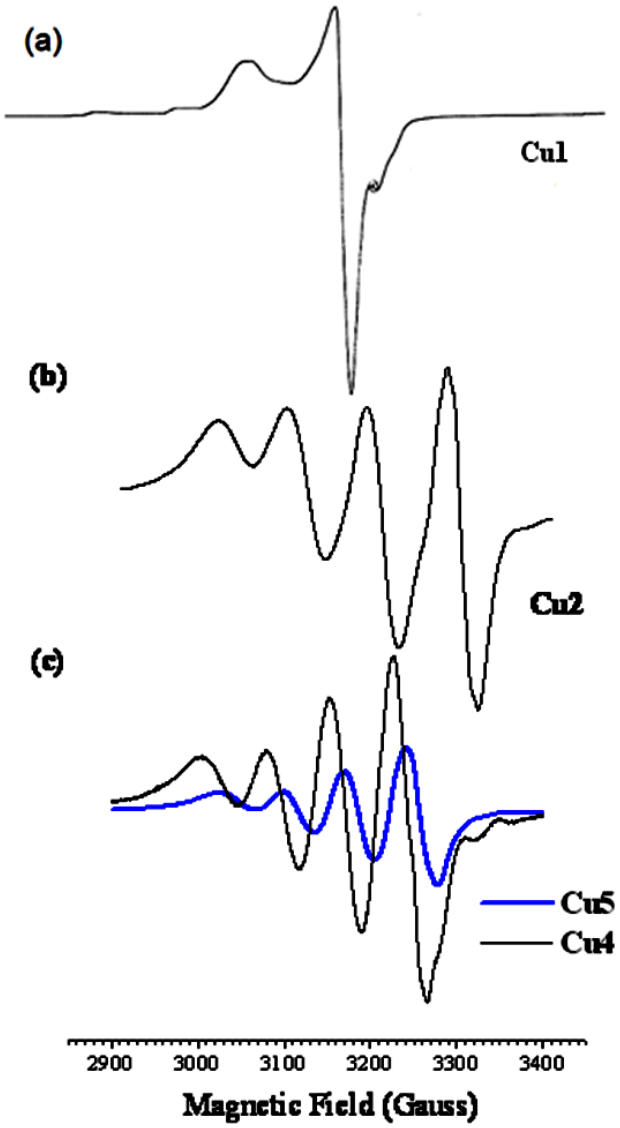

Figure 3.13 EPR spectra of Cu(II) complexes prepared in DCM (10 mM). Spectra were collected at Room temperature, ν_0 = 9.1 GHz. (a) **Cu1** (b) **Cu2** (c) **Cu4** and **Cu5**

Table 3.2 EPR spectral data of the complexes.

Copper complexes	g∥-2.0023	g⊥- 2.0023	A (cm^{-1})	α^2
Cu1	0.259	0.047	0.01980	0.869
Cu2	0.117	0.013	0.01985	0.715
Cu3	0.117	0.013	0.01985	0.715
Cu4	0.141	0.057	0.02112	0.792
Cu5	0.129	0.047	0.02035	0.754
Cu6	0.129	0.047	0.02035	0.754
Cu7	0.135	0.055	0.02105	0.787
Cu8	0.257	0.045	0.01975	0.865
Cu9	0.133	0.053	0.02100	0.783

3.3.8. Single Crystal X-Ray analysis

The structure elucidation of the Cu(II) Betti base complex was done with Single crystal X-Ray study. The crystallization of the metal complex was carried out by solvent diffusion method. The diethylether solvent was slowly layered on acetonitrile solution of the complex and allowed to stand. The single crystal X-Ray analysis of suitable crystal was done.

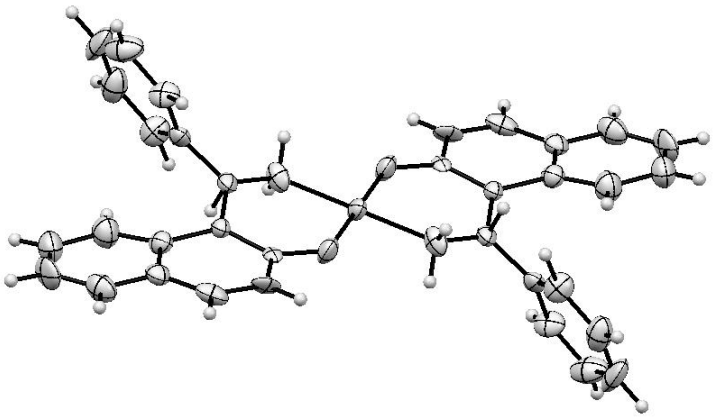

Figure 3.14 ORTEP diagram of **Cu1**

The ORTEP diagram of **Cu1** is shown in Figure 3.14. The crystal data for **Cu1** are given in Table 3.3 and selected bond lengths and angles are presented in Table 3.4. The copper atom is bonded to two nitrogen and two oxygen atoms; both pairs are in trans position with a perfect square planer geometry around copper. It is evident from the crystal structure that the two phenyl rings are positioned at opposite sides of the

molecular plane. Moreover the naphthyl rings are not strictly planar; they are slightly bent away from the phenyl rings with 174º instead of 180º as shown in Figure 3.14.

Table 3.3 Crystal Data for complex **Cu1**

Compound	complex
Emperical formula	$C_{34}H_{28}CuN_2O_2$
Formula mass	560.11
Temperature	293(2)K
Wavelength	0.71073 A
Crystal system	Monoclinic
Space group	$P2_1/c$
a [A]	14.964(16)
b [A]	5.763(6)
c [A]	20.524(16)
α [˚]	90
β [˚]	132.92(5)
Volume [$A^{\circ 3}$]	1296(2)
Z	2
Calculated density[Mg/m^3]	1.430
Absorption coefficient[mm^{-1}]	0.878
F(000)	578
Crystal size[mm]	0.28 × 0.14 × 0.05
θ-range[˚]	1.98 – 24.00
Index ranges	-17 ≤ h ≤ 15 -6 ≤ k ≤ 4 -23 ≤ I ≤ 22
Reflection collected/unique	5546/2043
Refinement method	Based on F^2
Data/restraints/parameters	2043/0/190
Goodness of fit on F^2	1.233
Final R indices [I>2σ(I)]	R1 = 0.1188 wR_2 = 0.2227
R indices (all data)	R1 = 0.1596 wR_2 = 0.2414
Largest diff. peak/hole [$eA^{\circ -3}$]	0.693/-0.741

Table 3.4 Selected bond lengths [Å] and angles [°] for complex **Cu1**

Cu-N1	1.90(1)
Cu-N1o	1.90(1)
Cu-O	1.925(7)
Cu-Oo	1.925(7)
N1-Cu-O1	89.6(4)
N1o-Cu-O1o	89.6(4)
N1-Cu-N1o	180.0(4)
O1-Cu-O1o	180.0(3)
Cu-O1-C1	129.2(7)
Cu-O1-C1o	129.2(7)
C10-C11-C12	122.0(1)
N1-C11-C12	115.65(1)

Efforts to crystallize Cu(II) complexes with optically active Betti base failed. Analysis of the EPR data for **Cu2** and **Cu3** stipulated us to anticipate a structure with more distortion around metal ion. The proposed structure is depicted in Figure 3.15. The distortion around metal ion may be due to both the phenyl rings lying on the same side of the molecular plane.

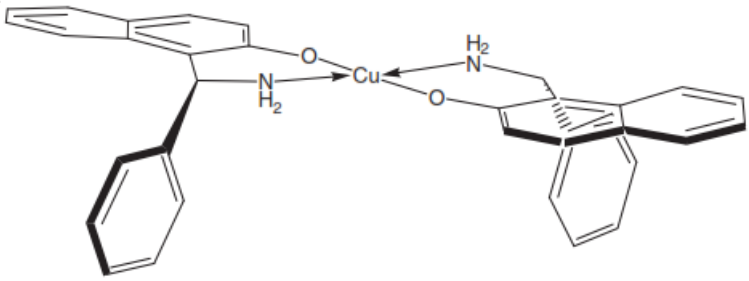

Figure 3.15 Proposed structure of **Cu2**

3.3.9. Electrochemical study

The electrochemical behavior of Cu(II) Betti base complexes in CH_2Cl_2 using $TBAPF_6$ as supporting electrolyte was investigated. The observed redox potentials for the complexes are tabulated in the Table 3.5.

Table 3.5 Electrochemical data[a] for copper(II) complexes at 25 ± 2 °C in DCM solution.

Complex	Ep_c (v)	Ep_a(v)
Cu1	–0.49	0.33
Cu4	–0.53	0.38
Cu7	–0.51	0.35
Cu8	–0.48	0.34
Cu9	–0.49	0.33

[a] Potential measured vs. Ag/Ag^+ reference electrode ; scan rate $50mVs^{-1}$; supporting electrolyte : $TBAPF_6$ (0.1M); complex concentration : 0.001M.

Figure 3.16 (a) shows the overlaid CVs for a solution containing 0.005 M **Cu2** and 0.05 M $TBAPF_6$ in DCM cycled at 10-40 mVs^{-1}. Two redox peaks were observed within the solvent stability window. The anodic peak was observed at 0.33 V while the cathodic peak was observed at -0.49 V. To check the cathodic peak $\mathbf{c_1}$ is due to reduction of metal center, CV was run in the potential window of 0.1 V to -0.6 V. As can be seen from the Figure 3.16 (b) reduction peak due to metal center was observed, as reduction of the ligand occurred only after its oxidized species was formed. So the cathodic peak was assigned for the reduction of Cu(II)→Cu(I) and anodic peak was assigned for the oxidation of the coordinated ligand. The oxidation potential of the coordinated ligand is shifted to less positive values compared to uncoordinated ligand, as expected on coordination to the metal ion. Similar results have been reported by other researchers working with similar systems. [5,11] A linear relationship is observed [Fig. 3.16(c-d)] between anodic/cathodic current and the square root of the sweep

rate, indicating both the processes to be diffusion controlled electrochemical process. [32]

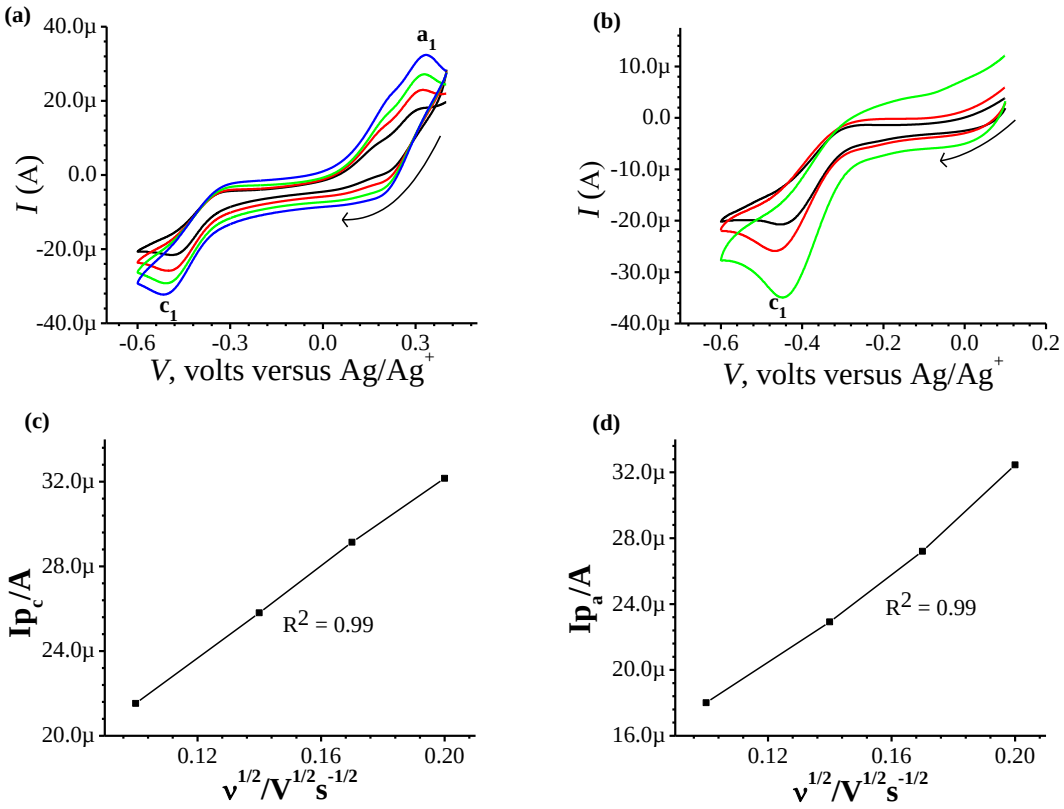

Figure 3.16 (a) and (b) cyclic voltammogram of **Cu2** with increasing scan rate 10 mV/sec to 40 mV/sec; (c) plot of the cathodic peak current for **Cu2** as a function of square root of scan rate in the range 10 mV to 50 mV/s. (d) plot of the anodic peak current for **Cu2** as a function of square root of scan rate in the range 10 mV to 50 mV/s.

The redox processes are irreversible as the anodic peak corresponding to electrochemical oxidation of Cu(I)→Cu(II) is not observed. The absence of anodic peak for the oxidation of Cu(I) could be due to intramolecular electron transfer via valence tautomerism between electroactive ligand and metal ion.[33-36] causing fast disproportionation of Cu(I) complex to give Cu(II) or some rearrangement within complex so as to give a more stabilized species.

To understand the redox process, elimination function E4 was applied to the CV data collected for **Cu2** at three scanning rates 10, 20 and 40 mV/sec. [37-40] The elimination function E4 for the oxidation process resulted in a prepeak at –0.5 V followed by broad doublet at 0.32 V as depicted in Figure 3.17(a). The application of

elimination function E4 for the reduction process resulted in a prepeak-peak **c_1' & c_1** as shown in Figure 3.17(b).

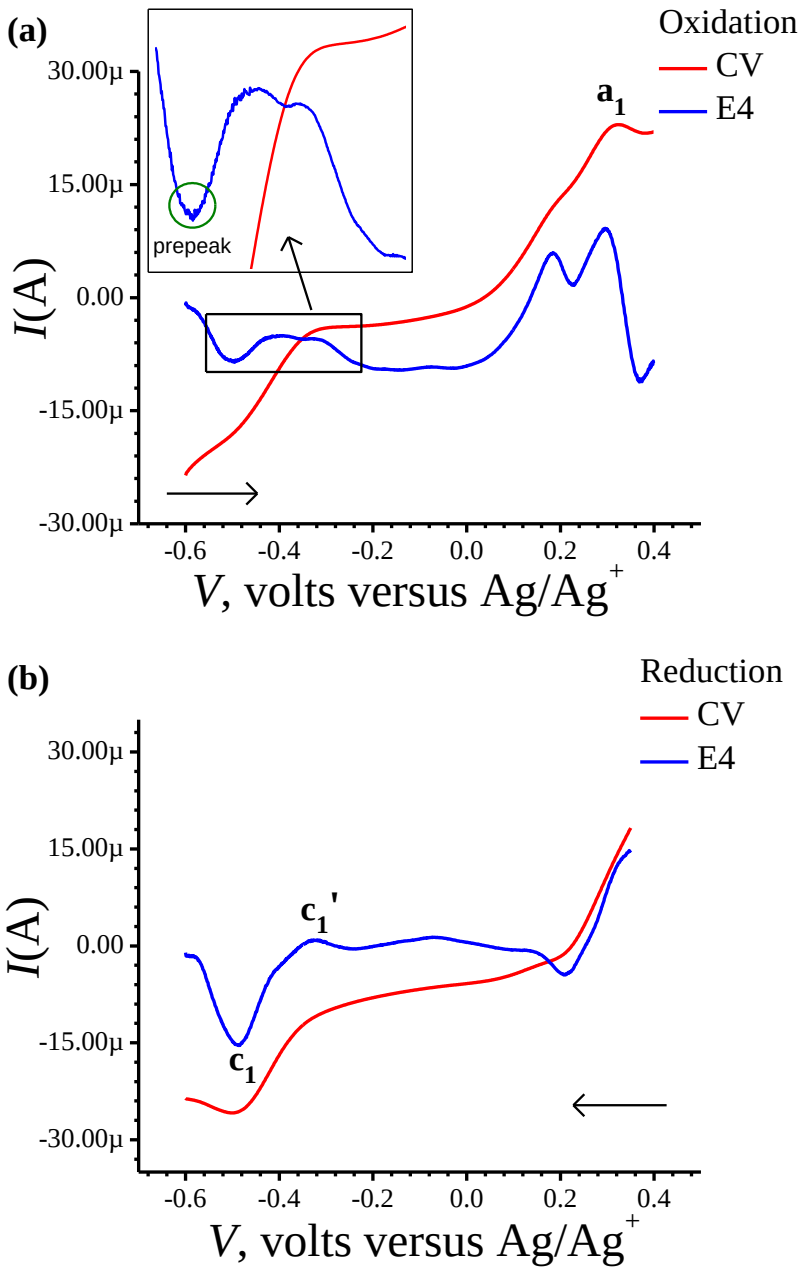

Figure 3.17 (a) E4 elimination plot for the oxidation of **Cu2** (b) E4 elimination plot for the reduction of **Cu2**.

The appearance of peak–counter peak with peak height lower than CV in the oxidation process **a_1** at 0.32 V [Fig. 3.17(a)] indicates diffusion controlled process of partially adsorbed species (For a completely adsorbed species the ratio should be 0.407). This is followed by reduction of the metal ion from Cu(II) to Cu(I) at **c_1** which

appears as prepeak – peak (**c_1'–c_1)** in EVLS [Fig. 3.17(b)] which indicates surface kinetics. The appearance of prepeak presumably due to change in geometry of the Cu(II) complex during reduction process. As can be seen from the voltammogram [Fig. 3.16(b)], the peak corresponding to oxidation of copper is not observed. This could be due to IET via valence tautomerism between electroactive ligand and metal ion [33-36] causing fast disproportionation of Cu(I) complex to give Cu(II) or some rearrangement within complex so as to give a more stabilized species. However the EVLS curves [Fig. 3.17(a)] exhibits prepeak followed by broad doublet indicates some chemical or a surface reaction prior to diffusion of the species. [40]

To understand nature of the process, E2 and E3 functions were also plotted for oxidation and reduction [Fig. 3.18(a-d)]. The increased peak height of **a_1** [Fig. 3.18(a)] in E2 indicates diffusion with the effect of kinetics whereas decreased or the distorted peak in the E3 function at **a_1** [Fig. 3.18(c)] indicates kinetic process as the diffusion current (I_d) is eliminated. Similar observation was obtained for the reduction process as well.

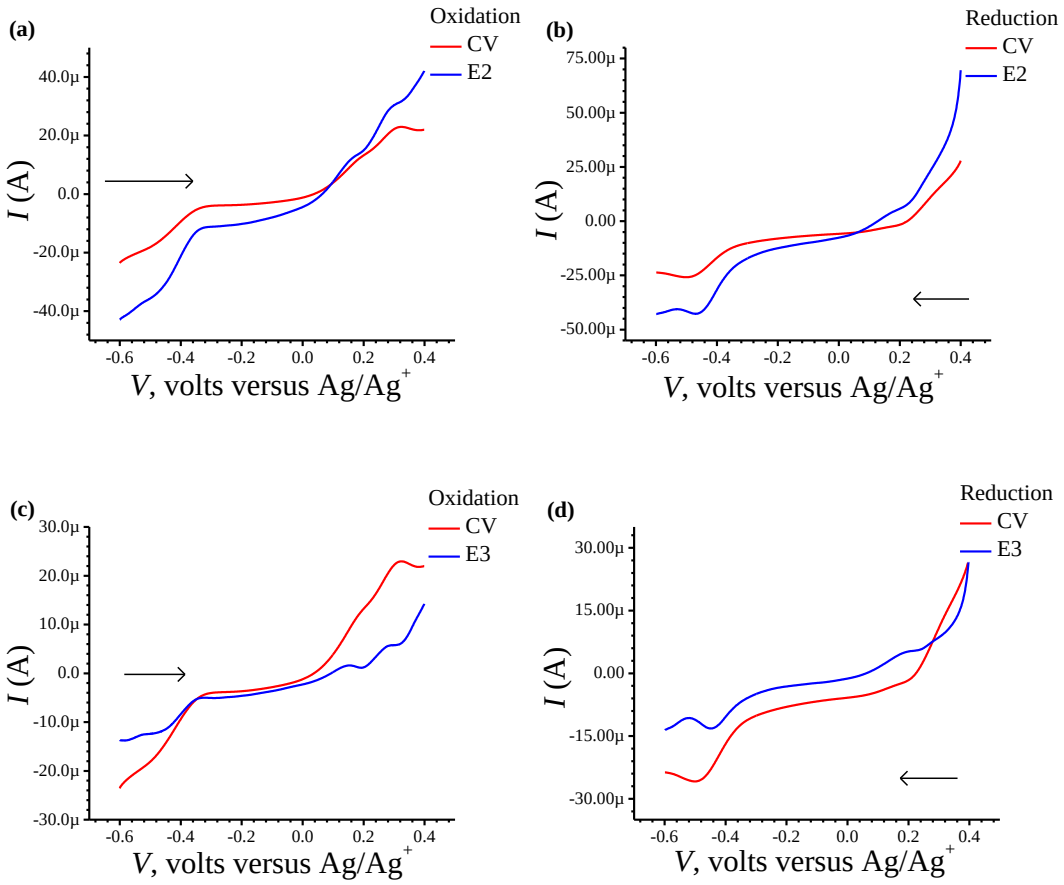

Figure 3.18 Plots for elimination functions **E2** (a) oxidation of **Cu2** (b) reduction of **Cu2** ; plots for the elimination function **E3** (c) oxidation of **Cu2** (d) reduction of **Cu2**

From the results obtained from CV and E4 curves, it can be proved that the **Cu2** complex follows ECE mechanism and the ligand is noninnocent in nature.

Figure 3.19 (a) shows the overlaid CVs for a solution containing 0.005 M **Cu5** and 0.05 M $TBAPF_6$ in DCM cycled at 100-500 mVs^{-1}. Similar CV as that of **Cu2** was obtained. Two redox peaks were observed within the solvent stability window. The anodic peak corresponding to oxidation of coordinated ligand was observed at 0.36 V while the cathodic peak corresponding to reduction of metal center was observed at -0.53 V. A linear relationship is observed [Fig 3.19(b)] between anodic/cathodic current and the square root of the sweep rate, which indicates both the processes are diffusion controlled electrochemical process. [32]

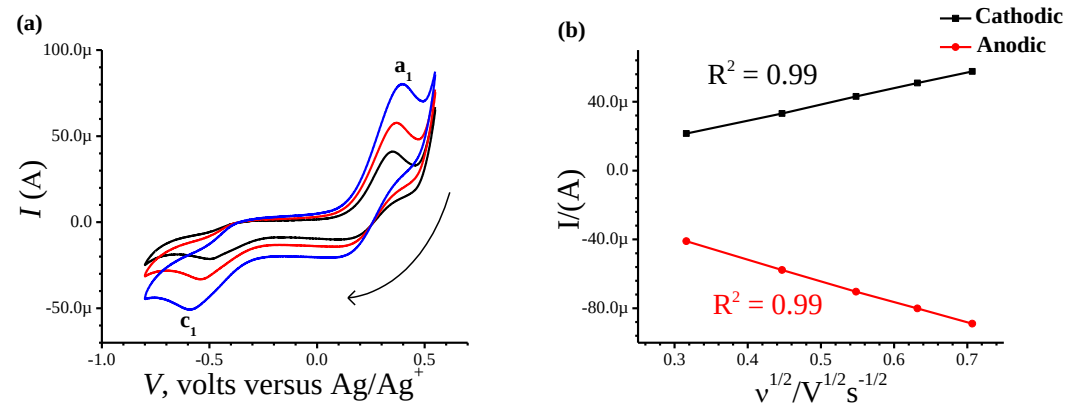

Figure 3.19 (a) cyclic voltammogram of **Cu5** with increasing scan rate 100 mV/sec to 400 mV/sec; (b) plot of the cathodic and anodic peak current for **Cu5** as a function of square root of scan rate in the range 100 mV to 500 mV/s.

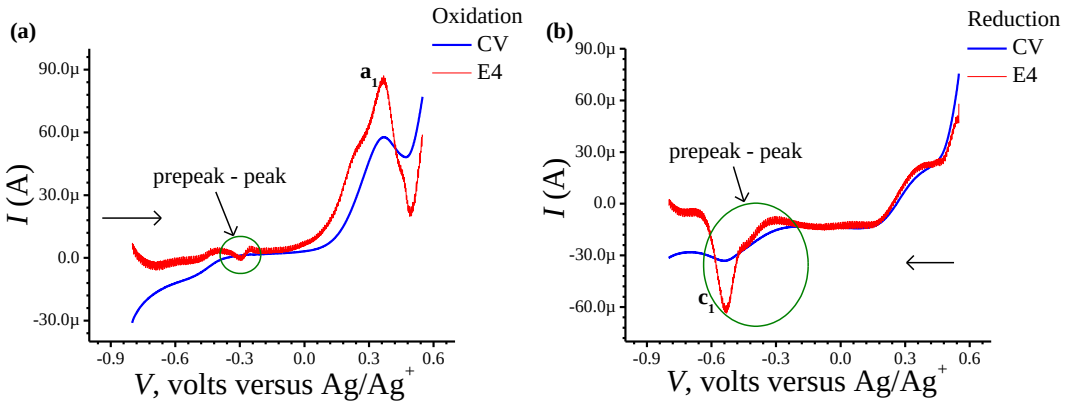

Figure 3.20 (a) E4 elimination plot for the oxidation of **Cu5** (b) E4 elimination plot for the reduction of **Cu5**.

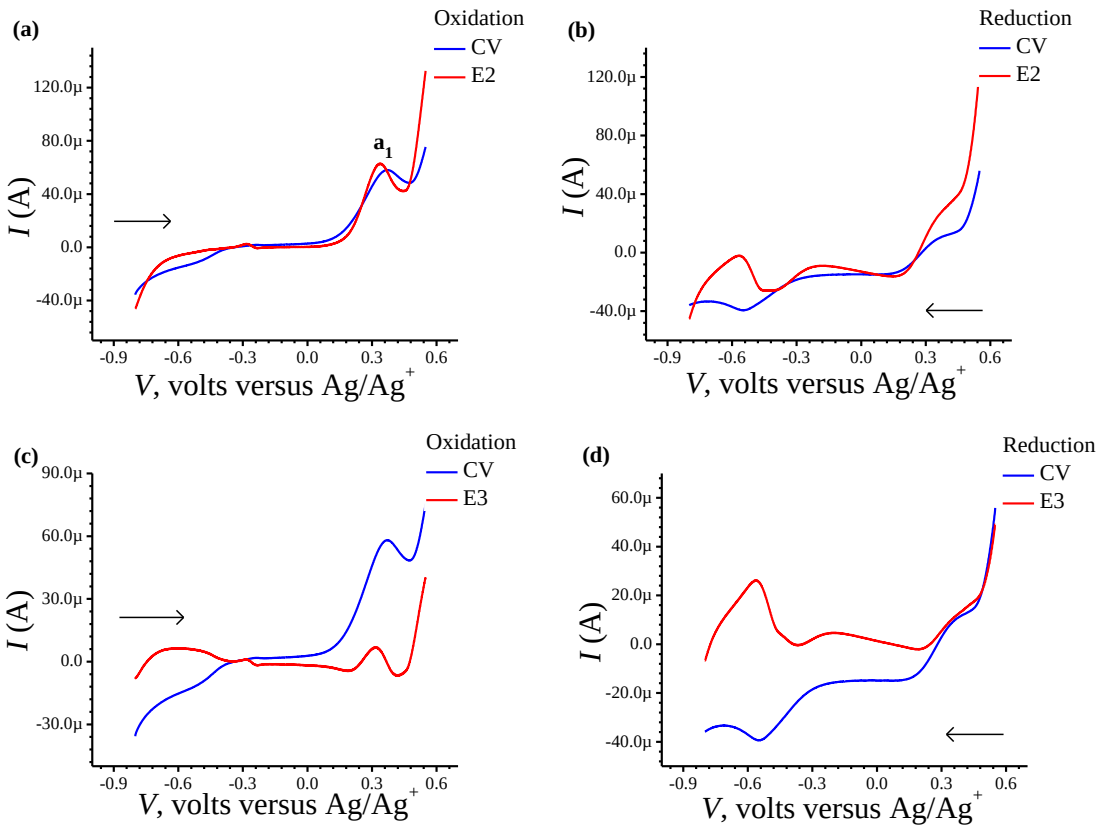

Figure 3.21 Plots for elimination functions **E2** (a) oxidation of **Cu5** (b) reduction of **Cu5** ; plots for the elimination function **E3** (c) oxidation of **Cu5** (d) reduction of **Cu5**

The elimination function E4 for the oxidation process resulted in a prepeak – peak at –0.3 V as depicted in Figure 3.20(a). Moreover the peak observed in CV at 0.37 V obtained with increase in height in E4 curve. The application of elimination function E4 for the reduction process resulted in a prepeak-peak **c_1' & c_1** as shown in Figure 3.20(b).

3.4. Conclusion

The reaction of amino naphthol ligands with Cu(II) in 1:2 mole ratio resulted in formation of $Cu(L\text{-}H)_2$ complexes. The geometry of Cu(II) complex with racemic composition of Betti base is square planar, with phenyl rings lying on opposite side of the molecular plane as confirmed by single crystal X-ray analysis. The geometry of the other complexes is speculated to be more distorted. The structure of complexes with optically active ligands has been proposed, which has two phenyl rings lying on the same side of the molecular plane, though in absence of XRD data, this could not be confirmed. The analysis of electrochemical data indicates ligand centered oxidation and metal centered irreversible reduction suggesting noninnocent behavior of the ligand.

3.5. Supporting information

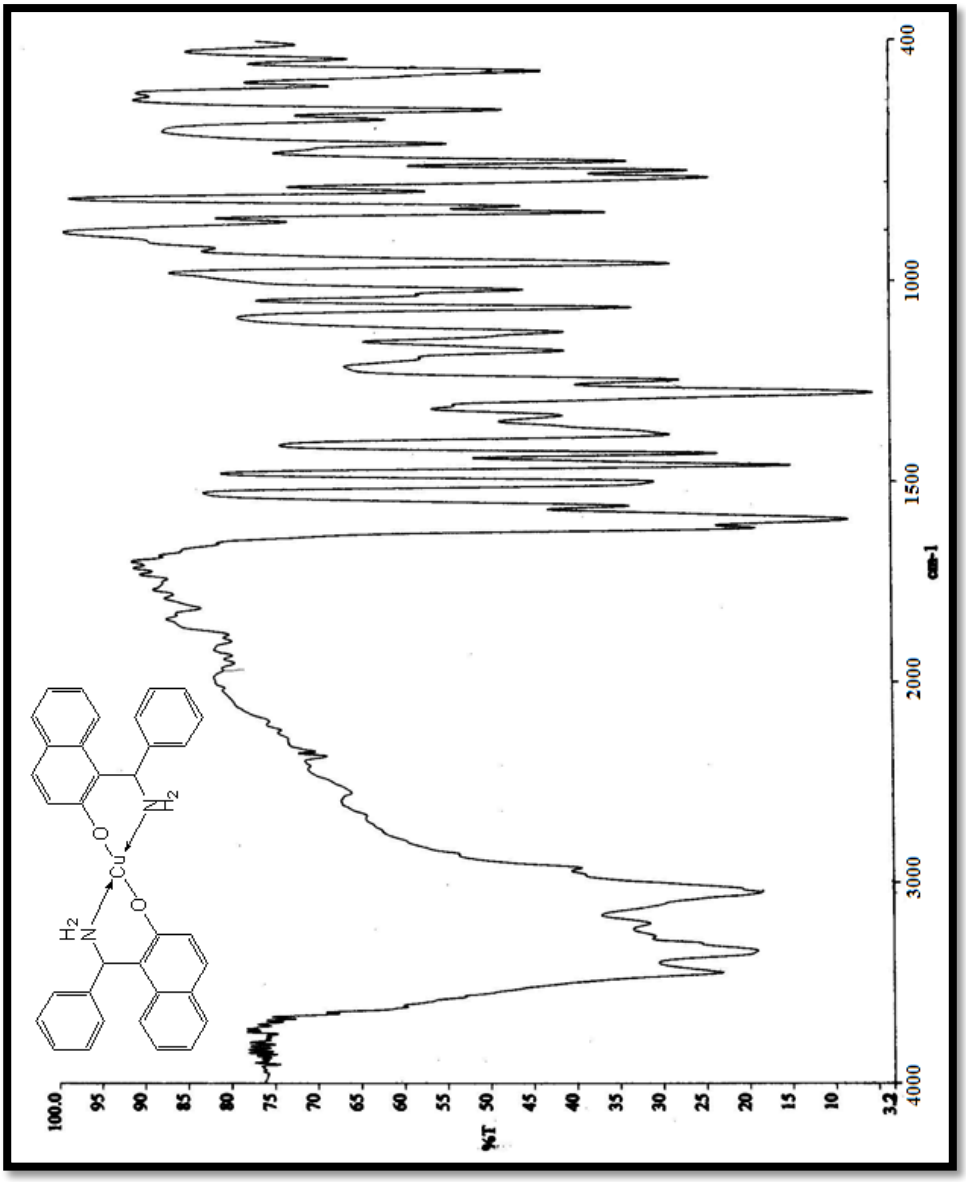

3.1SI FT-IR spectrum of CuBB

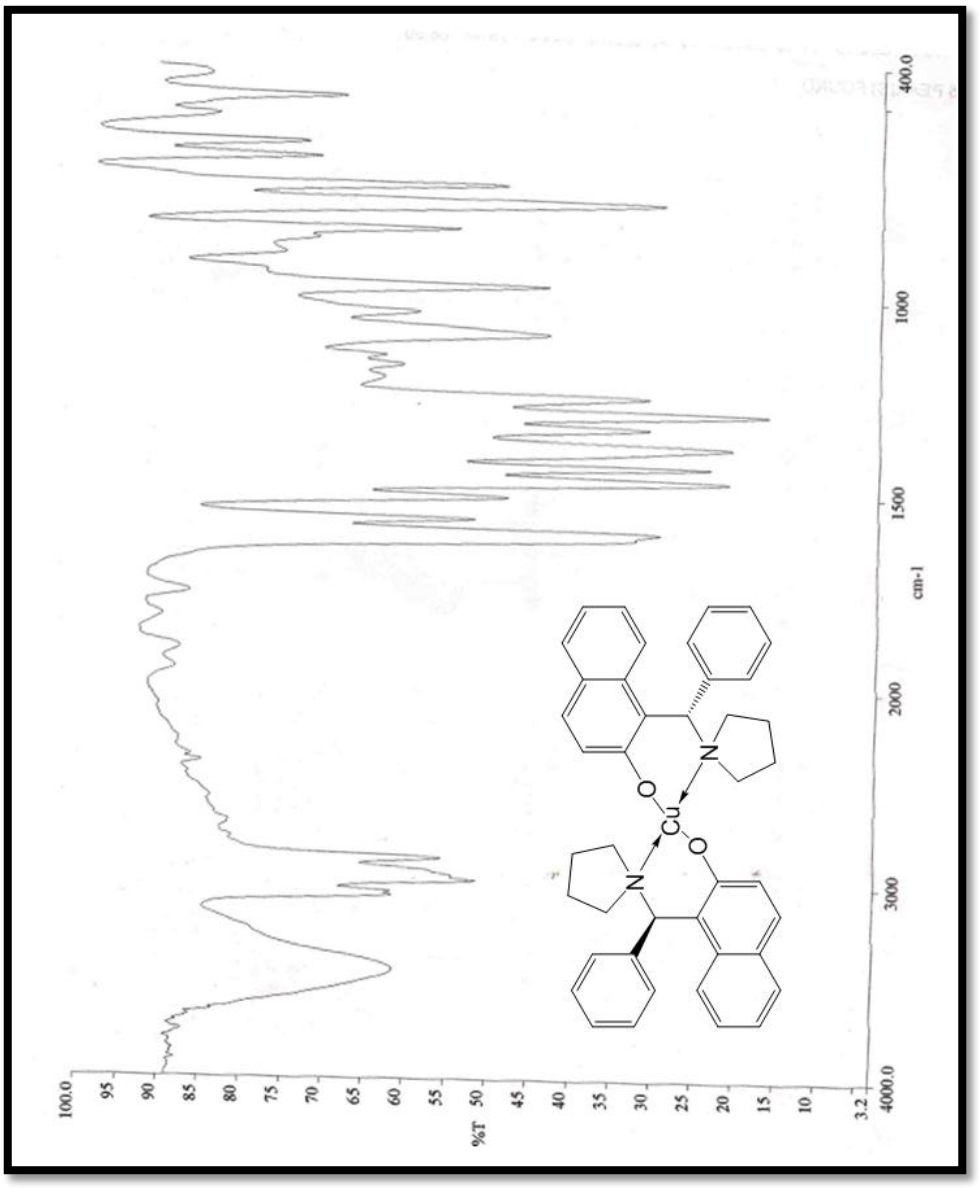

3.2SI FT-IR spectrum of CuPBB

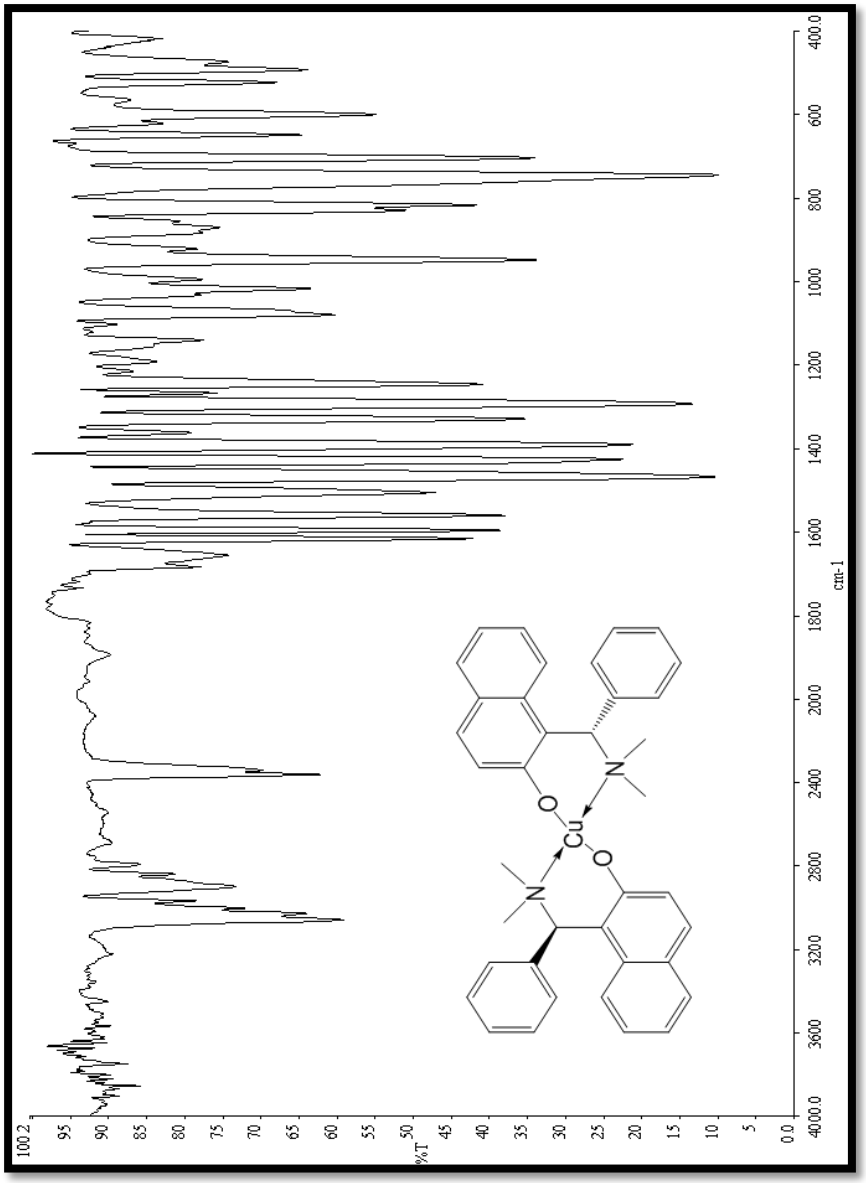

3.3SI FT-IR spectrum of CuDBB

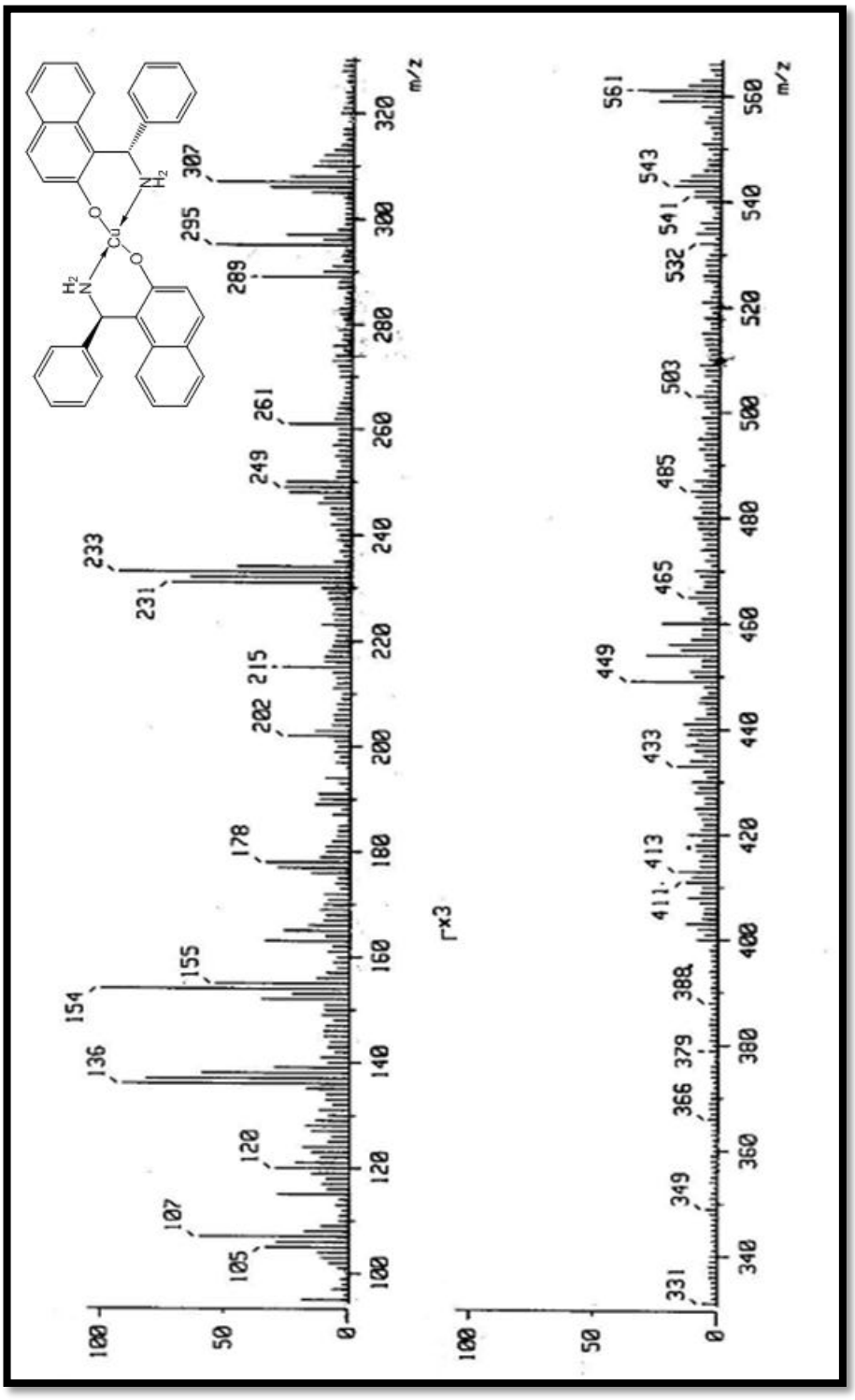

3.4SI FAB-Mass spectrum of CuBB

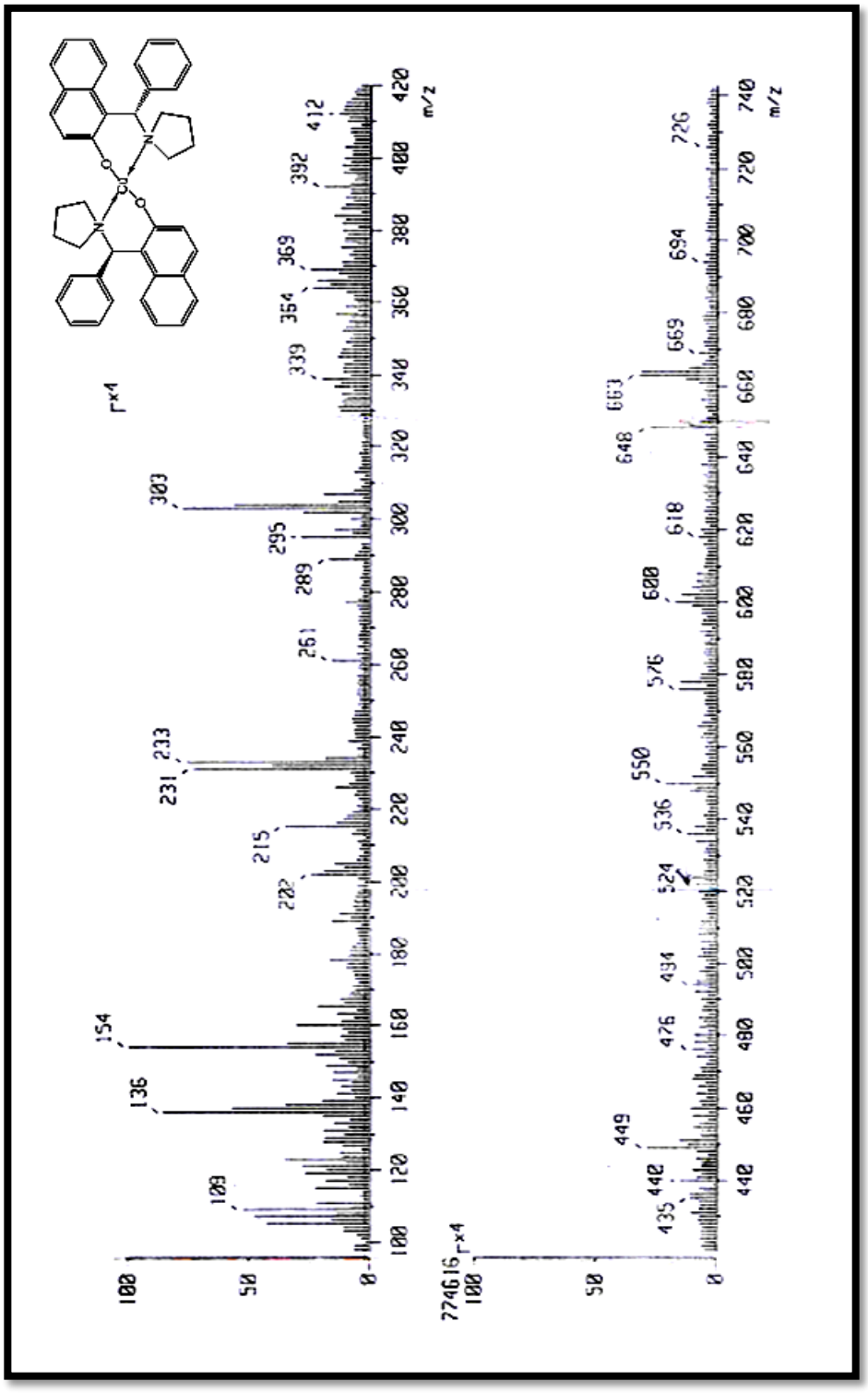

3.5SI FAB-Mass spectrum of CuPBB

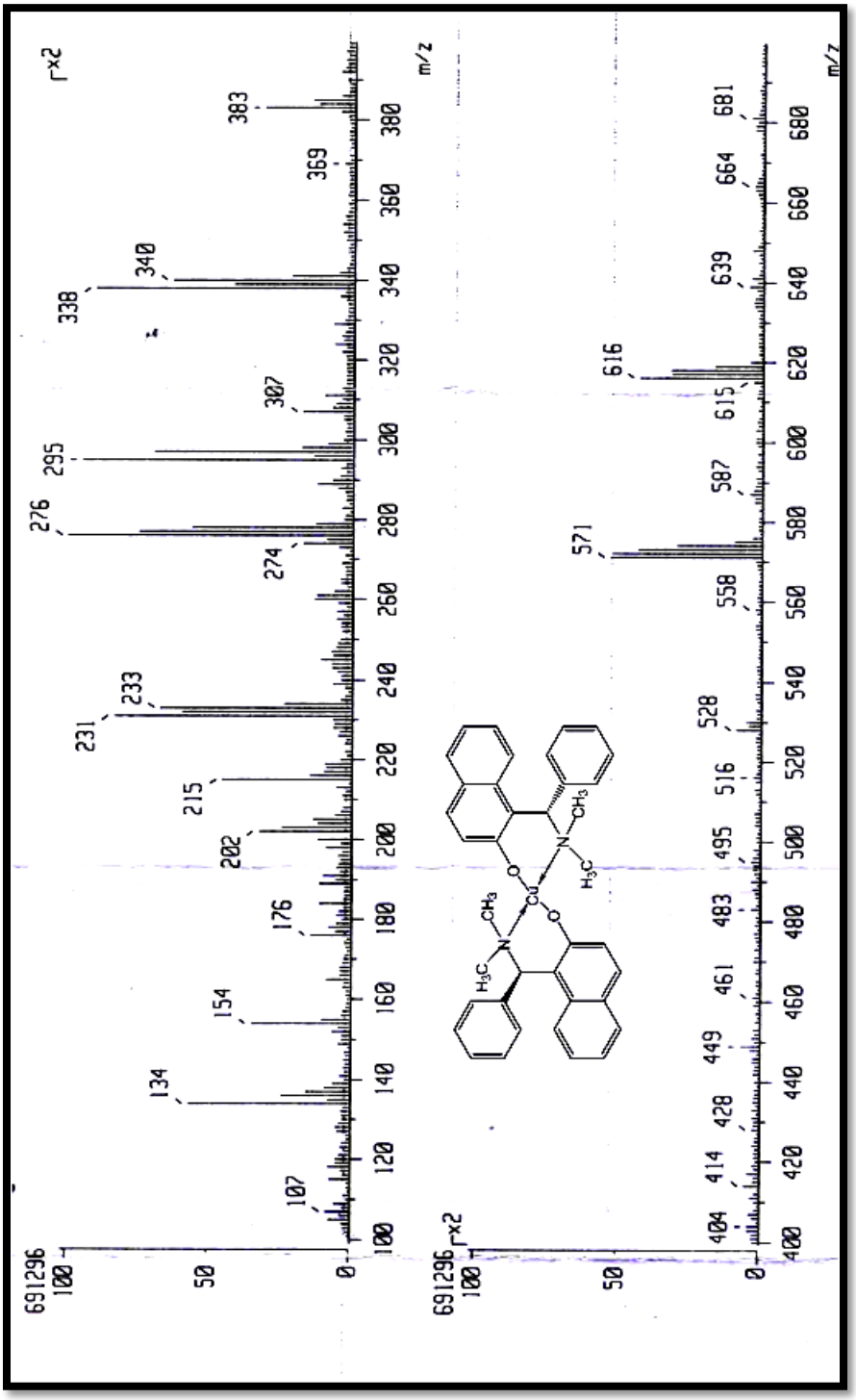

3.6SI FAB-Mass spectrum of CuDBB

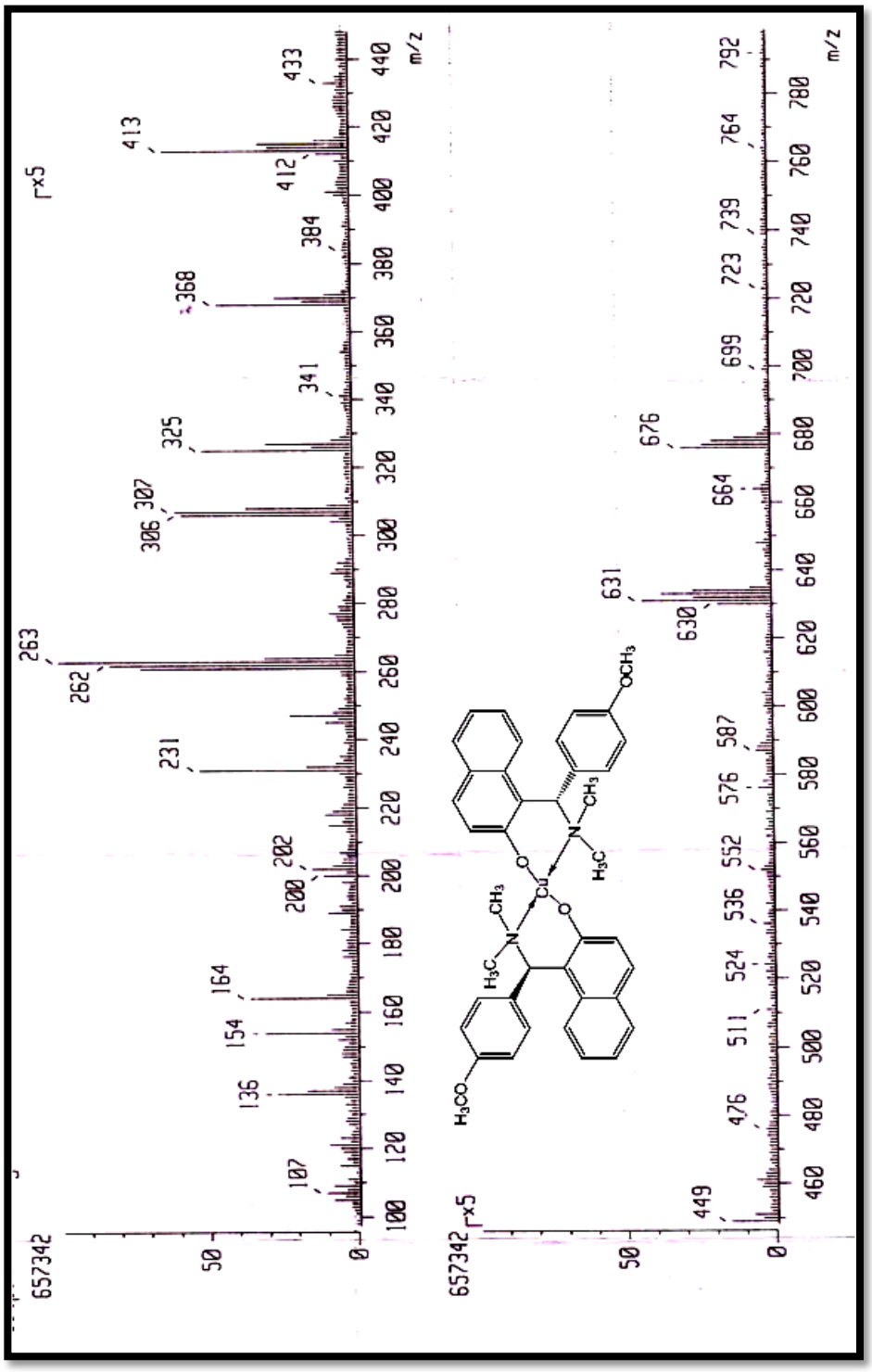

3.7SI FAB-Mass spectrum of CuADBB

3.6. References

[1] a) S. Turba, S.P. Foxon, A. Beitat, F.W. Heinemann, K. Petukhov, P. Muller, O. Walter, F. Lloret, M. Julve, S. Schindler, *Inorg. Chem.* **2012**, 51, 88−97; b) V.Kumar, A. Kalita, B. Mondal, *Dalton Trans*., **2013**, 42, 16264–16267; c) C. Adhikary, S. Banerjee, J. Chakraborty, S. Ianelli, *Polyhedron* **2013**, 65, 48–53; d) A. Seyed, H. Yazdi, P.S. Aghdam, A. Mirzaahmadi, A.A. Khandar, G. Mahmoudi, M. Ruck, T. Doert, S.S. Balula, L.C. Silva, *Polyhedron* **2014**, 80, 41–46.

[2] a) J. Manzur, H. Mora, V. Peredes Garcia, A. Vega, M.A. Novak, *Polyhedron* **2013**, 51, 180–185; b) A.A. Aziz, A.N.M. Salem, M.A. Sayed, M.M. Aboaly, *Journal of Molecular Structure* **2012**, 1010, 130–138.

[3] a) G.M. Chans, E. Gomez, V.G. Vidales, R.A. Toscano, C.A. Toledano, *Journal of Coordination Chemistry* **2015**, 68, 206–219; b) P. Adao, S. Barroso, M.F.N.N. Carvalho, C.M. Teixeira, M.L. Kuznetsov, J.C. Pessoa, *Dalton Trans*., **2015**, 44, 1612–1626.

[4] a) W. Kaim, *Dalton Trans.* **2003**, 761–768; b) J.W. Whittaker, *Chem. Rev.* **2003**, *103*, 2347–2363; c) T. K. Paine, T. Weyhermüller, K. Wieghardt, P. Chaudhuri, *Dalton Trans.* **2004**, 2092–2101; d) K. T. Sylvester, P. J. Chirik, *J. Am. Chem. Soc.* **2009**, *131*, 8772–8774; e) W. Kaim, B. Schwederski, *Coord. Chem. Rev.* **2010**, *254*, 1580–1588; f) A. L. Smith, K. I. Hardcastle, J. D. Soper, *J. Am. Chem. Soc.* **2010**, *132*, 14358–14360; g) W. I. Dzik, J. I. van der Vlugt, J. N. Reek, B. de Bruin, *Angew. Chem. Int. Ed.* **2011**, *50*, 3356–3358; h) O. Das, T. K. Paine, *Dalton Trans.* **2012**, *41*, 11476–11481.

[5] F. Thomas, *Eur. J. Inorg. Chem.* **2007**, 2379–2404

[6] B. A. Jazdzewski, W. B. Tolman, *Coord. Chem. Rev.* **2000**, *200*, 633–685.

[7] a) S. Itoh, M. Taki, S. Takayama, S. Nagatomo, T. Kitagawa, N. Sakurada, R. Arakawa, S. Fukuzumi, *Angew. Chem. Int. Ed.* **1999**, *38*, 2774–2776; *Angew. Chem.* **1999**, *111*, 2944–2946; b) L. Que, W. B. Tolman, *Nature* **2008**, *455*, 333–340; c) F. Himo, L. A. Eriksson, F. Maseras, P. E. Siegbahn, *J. Am. Chem. Soc.* **2000**, *122*, 8031–8036; d) P. Chaudhuri, M. Hess, U. Flörke, K. Wieghardt, *Angew. Chem. Int. Ed.* **1998**, *37*, 2217–2220; *Angew. Chem.* **1998**, *110*, 2340–2343; e) F. Thomas, G. Gellon, I.G. Luneau, E.S. Aman, J.L. Pierre, *Angew. Chem. Int. Ed.* **2002**, 41, 3047–3050.

[8] B. A. Jazdzewski, W. B. Tolman, *Coord. Chem. Rev.* **2000**, *200*, 633–685.

[9] A. Sokolowski, B. Adam, T.Weyhermüller, A. Kikuchi, K. Hildenbrand, R. Schnepf, P. Hildebrandt, E. Bill, K. Wieghardt, *Inorg. Chem.* **1997**, *36*, 3702–3710.

[10] E.H. Alilou, E. Amadei, M. Giorgi, M. Pierrot, M. Re´glier, *J. Chem. Soc. Dalton Trans*. **1993**, 549–557.

[11] P. Chaudhuri, K. Wieghardt, *Prog. Inorg. Chem*. **1988**, 35, 329–436.

[12] a) D. Hall, T.N. Waters, *J. Chem. Soc*. **1960**, 2644–2648; b) E.N. Baker, D. Hall, T.N. Waters, *J. Chem. Soc. (A)* **1970**, 406–409; c) M.B. Ferrari, G.G. Fava, C. Pelizzi, *Acta Crystallogr. Sect. B* **1976**, 32, 901–908; d) P. Cassoux, A. Gleizes, *Inorg. Chem.* **1980**, 19, 665–672.

[13] a) T.P. Cheeseman, D. Hall, T.N. Waters, *J. Chem. Soc. (A)* **1966**, 1396–1406; b) N. Galesic, R. Trojko, Z. Cimerman, Z. Stefanac, *Acta Crystallogr. C* **1984**, 40, 232–235; c) K. Bernardo, S. Leppard, A. Robert, G. Commenges, F. Dahan, B. Meunier, *Inorg. Chem*. **1996**, 35, 387–396.

[14] N. Kitajima, K. Whang, Y. Moro-oka, A. Uchida, Y. Sasada, *J. Chem. Soc. Chem. Commun.* **1986**, 1504–1505.

[15] a) Y. Wang, T.D.P. Stack, *J. Am. Chem. Soc*. **1996**, 118, 13097–13098; b) Y. Wang, J.L. DuBois, B. Hedman, K.O. Hodgson, T.D.P. Stack, *Science* **1998**, 279, 537–540.

[16] a) S. Trofimenko, *Chem. Rev.* **1993**, 93, 943–980; b) N. Kitajima, W.B. Tolman, *Prog. Inorg. Chem*. **1995**, 43, 419–531.

[17] T. Storr, P. Verma, R. C. Pratt, E. C. Wasinger, Y. Shimazaki, T. D. P. Stack, *J. Am. Chem. Soc.* **2008**, *130*, 15448–15459

[18] R. C. Pratt, C. T. Lyons, E. C. Wasinger, T. D. Stack, *J. Am. Chem. Soc.* **2012**, *134*, 7367–7377.

[19] a) Y. Wang, T. Stack, *J. Am. Chem. Soc.* **1996**, *118*, 13097– 13098; b) V. Mahadevan, R. Gebbink, T. D. P. Stack, *Curr. Opin. Chem. Biol.* **2000**, *4*, 228–234; c) C. Mukherjee, U. Pieper, E. Bothe, V. Bachler, E. Bill, T. Weyhermüller, P. Chaudhuri, *Inorg. Chem.* **2008**, *47*, 8943–8956; d) P. Chaudhuri, C. N. Verani, E. Bill, E. Bothe, T. Weyhermüller, K. Wieghardt, *J. Am. Chem. Soc.* **2001**, *123*, 2213–2223; e) L. Benisvy, A. J. Blake, D. Collison, E. S. Davies, C. D. Garner, E. J. L. McInnes, J. McMaster, G. Whittaker, C. Wilson, *Chem. Commun.* **2001**, 1824–1825; f) L. Benisvy, E. Bill, A. J. Blake, D. Collison, E. S. Davies, C. D. Garner, G.

McArdle, E. J. McInnes, J. McMaster, S. H. Ross, C. Wilson, *Dalton Trans.* **2006**, 258–267; g) S. E. Balaghi, E. Safaei, L. Chiang, E. W. Wong, D. Savard, R. M. Clarke, T. Storr, *Dalton Trans.* **2013**, *42*, 6829–6839.

[20] Z. Alaji, E. Safaei, L. Chiang, R.M. Clarke, C. Mu, T. Storr, *Eur. J. Inorg. Chem.* **2014**, 6066–6074.

[21] I. Szatmari, F. Fulop, *Curr. Org. Synth*. **2004**, 1, 155–165.

[22] C. Cimarelli, G. Palmieri, *Chirality* **2009**, 21, 218–232.

[23] G.M. Sheldrick, SHELXTL Reference Manual: Version 5.1, Bruker AXS, Madison,

WI, 1997.

[24] G.M. Sheldrick, SHELXL-97: Program for Crystal Structure Refinement, University

of Göttingen, Göttingen, 1997.

[25] S. Bayari, A. Atac, S. Yurdakul, *J. Mol. Struct*. **2003**, 655, 163–170.

[26] H. Elias, C. Hasserodt, L. Hellriegel, W. Schonherr, K. Wannowius, *Inorg. Chem*. **1985**, 24, 3192–3198.

[27] S. Zolezzi, A. Decinti, E. Spodine, *Polyhedron* **1999**, 18, 897–904.

[28] A. Pasini, M. Gullotti, R. Ugo, *J. Chem. Soc*., *Dalton Trans*. **1977**, 346–356.

[29] B.J. Hathaway, Copper, Comprehensive Coordination Chemistry, vol. 5, Pergamon Press, Oxford, 1987, p. 533.

[30] R.L. Dutta, A. Syamal, in: R.L. Dutta, A. Syamal (Eds.), Elements of Magnetochemistry, second ed., East–West Press, New Delhi, 1993, p. 47.

[31] D. Kivelson, R. Neiman, *J. Chem. Phys.* **1961**, 35, 149–155.

[32] A.J. Bard, L.R. Faulkner, Electrochemical Methods, Fundamentals and Applications, John Wiley & Sons, New York, 1980.

[33] E. Evangelio, D. Ruiz-Molina, *Comptes Rendus Chimie*, **2008**, 11, 1137–1154.

[34] E. Evangelio, D. Ruiz-Molina, *European Journal of Inorganic Chemistry*, **2005**, 15, 2957–2971.

[35] O.Rotthaus, F.Thomas, O. Jarjayes,C.Philouze, E. Saint-Aman, J.-L. Pierre, *Chemistry: A European Journal* **2006**, 12, 6953–6962.

[36] W. Kaim, B. Schwederski, *Pure and Applied Chemistry* **2004**, 76, 351–364.

[37] O. Draˇcka, *Journal of Electroanalytical Chemistry* **1996**, 402, 19–28

[38] L. Trnkov´a, O. Draˇcka, *Journal of ElectroanalyticalChemistry* **1996**, 413, 123–129

[39] L. Trnkov´a, F. Jelen, I. Postbieglov´a, *Electroanalysis* **2003**, 15, 1529–1535.

[40] L. Trnkov´a, *Journal of Electroanalytical Chemistry* **2005**, 582, 258–266.

[41] a) G. Pandey, S. Pal, R. Laha, *Angew. Chem.* **2013**, 125, 5250–5253; *Angew. Chem. Int. Ed.* **2013**, 52, 5146–5149; b) C.J. Li, *Acc. Chem. Res*. **2009**, 42, 335–344; c) P. Xie, Y. Xie, B. Qian, H. Zhou, C. Xia, H. Huang, *J. Am. Chem. Soc.* **2012**, 134, 9902–9905; d) Z. Li, Li. Cao, C.-J. Li, *Angew. Chem.* **2007**, 119, 6625–6627; *Angew. Chem. Int. Ed*. **2007**, 46, 6505–6507; e) Z. Li, C. J. Li, *J. Am. Chem. Soc.* **2005**, 127, 3672–3673.

[42] a) S.J. Park, J.R. Price, M.H. Todd, *J. Org. Chem.* **2012**, 77, 949–955; b) L. Liu, P. E. Floreancig, *Angew. Chem*. **2010**, 122, 6030–6033; *Angew. Chem. Int. Ed.* **2010**, 49 5894–5897; c) B. Yu, T. Jiang, Y. Su, X. Pan, X. She, *Org. Lett.* **2009**, 11, 3442–3445; d) Y. Zhang, C. J. Li, *J. Am. Chem. Soc*. **2006**, 128, 4242–4243.